Bioorganic Chemistry 45 (2012) 12–28

Contents lists available at SciVerse ScienceDirect

Bioorganic Chemistry

journal homepage: www.elsevier.com/locate/bioorg

Discovery of novel glitazones incorporated with phenylalanine and tyrosine: Synthesis, antidiabetic activity and structure–activity relationships ☆

B.R. Prashantha Kumar [a], Nasir R. Baig [b], Sai Sudhir [b], Koyal Kar [a], M. Kiranmai [c], M. Pankaj [c], Nanjan M. Joghee [c,*]

[a] Department of Pharmaceutical Chemistry, JSS College of Pharmacy, Mysore 570 015, India
[b] Department of Organic Chemistry, Indian Institute of Science, Bangalore 560 012, India
[c] TIFAC CORE, JSS College of Pharmacy, Ootacamund 643 001, India

ARTICLE INFO

Article history:
Received 19 March 2012
Available online 23 August 2012

Keywords:
CoMSIA
Dexamethazone
Glitazones
Glucose uptake activity
Insulin resistance
Thiazolidinediones

ABSTRACT

We report a series of new glitazones incorporated with phenylalanine and tyrosine. All the compounds were tested for their *in vitro* glucose uptake activity using rat-hemidiaphragm, both in presence and absence of insulin. Six of the most active compounds from the *in vitro* screening were taken forward for their *in vivo* triglyceride and glucose lowering activity against dexamethazone induced hyperlipidemia and insulin resistance in Wistar rats. The liver samples of rats that received the most active compounds, **23** and **24**, in the *in vivo* studies, were subjected to histopathological examination to assess their short term hepatotoxicity. The investigations on the *in vitro* glucose uptake, *in vivo* triglyceride and glucose lowering activity are described here along with the quantitative structure–activity relationships.

© 2012 Elsevier Inc. All rights reserved.

1. Introduction

Type 2 diabetes mellitus, considered today as a life-style disease, is usually associated with urbanization, mechanization, change in life style habits and caloric imbalance. Over 90% of the diabetes mellitus patients are of type 2 patients across the world [1]. Type 2 diabetes is a chronic disease characterized by hyperglycemia due to insulin resistance in the liver and peripheral tissues, or due to a defect in pancreatic β-cells or both [2,3]. The insulin resistance state at the peripheral level causes impaired glucose utilization leading to hyperglycemia, which is believed to play a role in the etiology of a wide spectrum of metabolic disorders such as obesity, hypertension, atherosclerosis, neuropathy, nephropathy, and retinopathy [4,5]. The conventional therapy of type 2 diabetes mellitus using sulphonylureas and biguanides has not been satisfactory as it is not successful in treating associated cardiovascular risk factors, a major cause of morbidity. Traditional treatment strategies include several oral hypoglycemic agents but practically none of these agents maintain glucose levels indefinitely. Many of the patients, therefore, require exogenous insulin therapy. The current trend is, therefore, to make therapy better by choosing appropriate combination of available drugs.

In the year 1999, troglitazone, a new class of drug called 'glitazone' or thiazolidinedione (TZD) was approved by the US FDA for the treatment of type 2 diabetes. It was, however, withdrawn later due to severe hepatotoxicity. Rosiglitazone and pioglitazone introduced later were marketed under regular monitoring and account for 21% of oral antidiabetic drugs used in the USA [6,7]. Glitazones correct hyperglycemia by enhancing tissue sensitivity to insulin. Glitazones are not associated with dangerous hypoglycemic incidents that are observed with conventional sulfonylureas and insulin therapy. Glitazones, however, are known to have cardiovascular risks in association with fluid retention and weight gain [8–13]. Identification and development of newer drugs from this class is, therefore, the need of the hour.

Glitazones are the agonists for the peroxisome proliferator activating receptors-γ (PPAR-γ), which regulate the transcription of insulin-responsive genes involved in the control of glucose production, transport and utilization [14]. PPAR-γ is a member of the subfamily, which belongs to a 48 member nuclear receptor super family [15–17]. A large number of insulin sensitizers have been synthesized and tested for their antidiabetic activity. Many of the candidate compounds have reportedly entered clinical studies. Some of these belong to the glitazone class, but others have different chemical structures with clofibrate and tyrosine moieties, etc. [18–22]. The majority of TZD containing antidiabetic agents reported in literature have a polar TZD ring system as a head followed by hydrophobic benzyloxy moiety as their trunk which is in turn connected to the hydrophobic tail via a two carbon linker

☆ *Author contributions*: Authors have equally contributed for the science and in editing this manuscript.

* Corresponding author. Fax: +91 4232447135.
E-mail address: mjnanjan@gmail.com (N.M. Joghee).

0045-2068/$ - see front matter © 2012 Elsevier Inc. All rights reserved.
http://dx.doi.org/10.1016/j.bioorg.2012.08.002

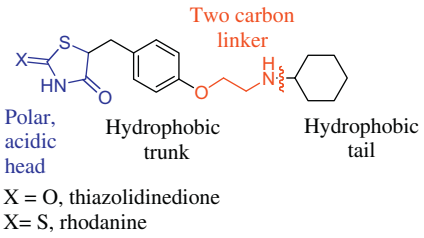

Fig. 1. Traditional pharmacophore structural part of glitazones.

(Fig. 1) [23,24]. Though the majority of TZD containing glitazones possess a methylene group bridged to the TZD and phenyl group, it has been shown by us and others independently that compounds with 5-benzylidene TZDs can also act as insulin sensitizers. Further, replacing TZD head with its bioisostere rhodanine ring has also been shown to retain activity to considerable levels [24,25].

2. Chemistry

Considering the above structural features of glitazones and with the objective of further probing the structure–activity relationships (SAR), we designed structures of some novel glitazones incorporated with phenylalanine and tyrosine residues. The hypothesis here is that, the amino acid moiety will increase the polarity and acidity near the thiazolidine ring due to the freely exposed carboxyl group and is also relatively safe with respect to its metabolism in the body. The synthesis of the title compounds incorporated with amino acids, phenylalanine and tyrosine were, therefore, carried out according to Scheme 1 to obtain compounds **5–20** and Scheme 2 to obtain compounds **23**–**28**.

We have selected two water soluble hydrophobic amino acids such as phenylalanine and its counterpart, tyrosine, as building blocks (Scheme 1). The amino acid was first converted to the corresponding ammonium salt and then reacted with carbon disulfide to yield the corresponding dithiocarbamates (**1** and **2**). The

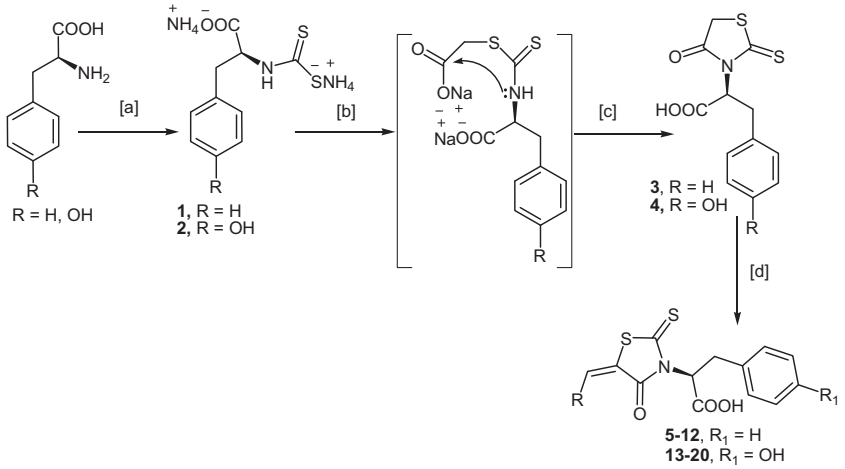

Scheme 1. Synthesis of 2-thioxo-thiazolidine-4-one derivatives incorporated with phenylalanine and tyrosine residues: (a) H_2O, 0–5 °C, aqueous ammonia solution 25–30%, CS_2, stir for 10 h; (b) 5–10 °C, sodium chloroacetate solution; (c) 6 N HCl, two drops $POCl_3$, 60–70 °C for 3 h; (d) toluene, subst aldehyde, piperidine or *N*-methyl piperazine, acetic acid, molecular sieves, reflux, 110 °C for 15 h or MW irradiation 700 W, 30 min.

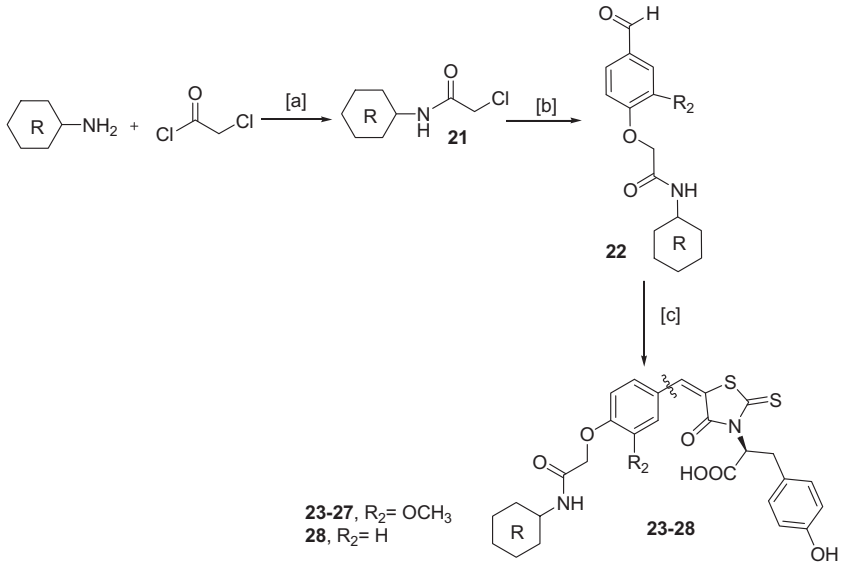

Scheme 2. Synthesis of glitazones **4**–**18**: (a) $CHCl_3$, Et_3N, 0–5 °C to rt, stirred for 6 h; (b) acetone, vanillin, K_2CO_3, stirred at rt 36 h; (c) toluene, **4**, *N*-methyl piperazine, ammonium acetate, molecular sieves, reflux at 110 °C for 15 h or MW irradiation 700 W, 30 min.

dithiocarbamates were then reacted with sodium chloroacetate followed by cyclization under acidic conditions in presence of phosphorous oxychloride to yield products in which the *N*-terminal of the amino acid is converted to the corresponding 2-thioxo-thiazolidine-4-ones, **3** and **4**. Compounds **3** and **4** were then subjected to the Knoevenagel condensation with aryl aldehydes, using *N*-methyl piperazine and ammonium acetate in refluxing toluene, to yield compounds **5**–**12** and **13**–**20** as listed in Table 1. Knoevenagel condensation was performed on **3** and **4**, using both conventional and microwave methods without the aid of Dean–Stark apparatus.

Apart from good yields, we have not obtained the same results contrary to the results reported by Wang et al. and Hardej et al. [26]. The present method is simple and easy. Here, we have prepared ammonium salt of dithiocarbamate rather sodium salt and the reaction completes at room temperature itself without heating. We also observed that the dithiocarbamates are relatively more stable under cold conditions. Phosphorous oxychloride along with HCl was found to be useful in the cyclization step, as it enhances the yields. The rate of Knoevenagel condensation with aldehydes over the active methylene group has been shown to increase when *N*-methyl piperazine and ammonium acetate are used, rather than piperidine and acetic acid mixture, under similar conditions [27].

The tail part was first synthesized by connecting various aromatic/alicyclic amines to the two carbon linker (Scheme 2). The acylated amines **21** were then connected to the *p*-hydroxy group of vanillin to obtain **23–27** and to *p*-hydroxy benzaldehyde to obtain **28**. Vanillin was used because it is a natural product and there are not many reports in literature about glitazones incorporated with a natural product like vanillin as part of their trunk [24]. The trunk, which is connected with the hydrophobic tail via the two carbon linker, was then connected to the head group, namely, 2-thioxo-thiazolidine-4-one or rhodanine ring system of **4** by adopting the Knoevenagel condensation reaction as described under Scheme 1.

The structures of the synthesized compounds were confirmed by IR, Mass and NMR analysis. The peak at around 7.6 δ ppm in ^{1}H NMR spectra and the signal between 130 and 135 δ ppm in ^{13}C NMR spectra confirm the =CH at the fifth position of thiazolidine ring system. The reason for this deshielding is attributed to the cis-position of the carbonyl function of 2-thioxo-thiazolidine-4-one ring to the =CH and hence the *Z* configuration [27,28]. *Cis* positioning is due to a high degree of thermodynamic stability of these compounds because of the intramolecular hydrogen bonding that are formed between the hydrogen atom of the =CH and the oxygen atom in the 2-thioxo-thiazolidine-4-one ring [29].

3. Results and discussion

3.1. Glucose uptake by in vitro rat hemi-diaphragm

The antidiabetic activities of the 24 synthesized compounds were measured using glucose uptake by rat hemi-diaphargm according to the method described by Walaas and Chattopadhyay [30,24]. The institutional animal ethics committee (IAEC) of JSS College of Pharmacy, Ootacamund, India, approved the proposal. Rat diaphragm was selected because the striated muscle is quantitatively the most important tissue for glucose disposal in the animal body. The glucose content was measured and the glucose uptake was calculated as the difference between the initial and final glucose content. Data were expressed as mean ± standard error of mean (SEM) and shown in Table 1.

Statistical comparisons between the groups were performed in two sets using one-way ANOVA followed by Dunnet's multiple comparison post-test using graphPad Prism 4.0 software for Windows (San Diego, California, USA). In the first set, group 1 that served as the control, was compared with groups (3–27) that are studied in the absence of insulin including the analogous standard drug (rosiglitazone). In the second set group 2 that served as the control, was compared with groups (3–27) that are studied in the presence of insulin. We neither compared set one versus set two groups nor all the groups with each other, as it is well known biologically that insulin enhances the glucose uptake. The focus was, therefore, to compare the differences made by the presence of compounds. A reasonable correlation between these two set of groups indicate some degree of correlation for the compounds with respect to their glucose uptake enhancement in the absence and presence of insulin. The results of the *in vitro* glucose uptake study indicate that all the compounds enhance the glucose uptake by the tissue from weak to moderate and from moderate to significant glucose levels. The results also reveal one key aspect, namely, the compounds significantly enhance the glucose uptake in the presence of insulin rather than in the absence of external insulin. It is evident, therefore, that this class of compounds tends to sensitize the tissue to take up insulin which enhances the glucose utilization by the tissue cells [31,32].

We have also investigated the structure–activity relationships based on the results obtained. Compounds **3** and **4** (which lack substitution at the 5th position of thiazolidine ring system) do not exhibit good activity, indicating that substitution at the 5th position of thiazolidine ring system is essential. Compounds **6** and **9** exhibit reasonably good glucose uptake activity, whereas the rest of the compounds incorporated with phenylalanine do not. Interestingly, compounds which are incorporated with tyrosine exhibit significant activity, especially, compounds **15**, **17**, **23**, **24**, **25**, **27** and **28** ($P < 0.01$). These compounds exhibit comparable glucose uptake activity when compared to the standard drug (rosiglitazone). Compounds **23**, **24**, **25**, **27** and **28** contain vanillin as their trunk, followed by two carbon acyl linker and hydrophobic tail in their structures. Compound **26** ($P < 0.05$) with one carbon linker exhibits moderate activity.

3.2. In vivo antihyperglycemic activity

Serum glucose and triglyceride lowering activity of the six most active compounds and the standard drug (rosiglitazone), were tested at a dose of 10 mg/kg, p.o. against dexamethasone induced hyperlipidemia and insulin resistance in Wistar rats [33]. Dexamethazone being a glucocorticoid, is well known for inducing obesity and insulin resistance in both animals and human beings [34,35]. On the day 11 of treatment, blood was collected for the estimation of serum glucose and triglyceride levels. The results of *in vivo* antihyperglycemic activity of the test compounds **15**, **23**, **24**, **25**, **27** and **28** are shown in Table 2.

3.2.1. Effect on serum glucose level

Except compound **28**, all the compounds at a dose of 10 mg/kg, p.o. significantly decrease the dexamethasone induced elevation of serum glucose. Standard rosiglitazone also significantly ($P < 0.01$) decrease the dexamethasone induced elevation of serum glucose. Among the six compounds tested, compound **23** show good antihyperglycemic activity superior to rosiglitazone. Compounds **24**, **27** and **25** also show significant glucose lowering activity ($P < 0.01$) in the descending order. Compound **15** shows good activity ($P < 0.05$). Compound **28** shows weak activity.

3.2.2. Effect on serum triglyceride level

Out of the six compounds and rosiglitazone tested, rosiglitazone, compounds **25**, **23**, **27** and **24** show significant triglyceride lowering activity ($P < 0.01$) as compared to the dexamethasone

Table 1
Glitazones and their effect on glucose uptake by the isolated rat hemi-diaphragm.

Cpd. no. (group no.)	R	Glucose uptake (mg/g/45 min)		CoMSIA	
		No insulin	With insulin	−ln MGU	Pred. act
3 (3,28)	–	9.86 ± 0.97	26.82 ± 1.80	2.3492	2.38
4 (4,29)	–	10.40 ± 0.96	28.03 ± 0.92	2.3604	2.332
5 (5,30)	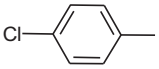	9.90 ± 0.82	27.77 ± 2.32	2.6749[a]	2.672[a]
6 (6/31)	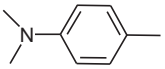	10.04 ± 1.04	29.32 ± 1.66	2.6427	2.63
7 (7,32)	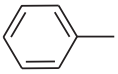	10.06 ± 1.34	27.51 ± 1.71	2.5962	2.612
8 (8,33)	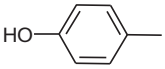	10.70 ± 0.50	28.84 ± 1.70	2.5914	2.592
9 (9,34)	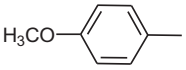	10.32 ± 0.91	29.28 ± 1.25	2.612	2.618
10 (10,35)	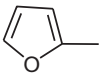	9.04 ± 0.93	26.16 ± 1.18	2.619	2.603
11 (11,36)	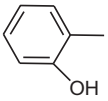	9.69 ± 1.15	27.79 ± 0.88	2.6285	2.619
12 (12,37)	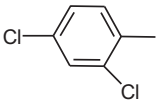	9.33 ± 0.91	26.30 ± 1.53	2.8103	2.798
13 (13,38)	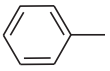	10.55 ± 0.91	29.87 ± 1.73	2.5563[a]	2.668[a]
14 (14,39)	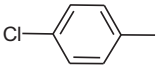	10.72 ± 1.00	30.39 ± 1.47	2.6237	2.661
15 (15,40)	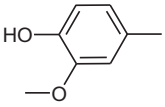	11.56 ± 2.15	33.95 ± 2.11**	2.5412	2.535
16 (16,41)	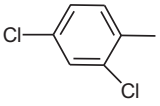	10.55 ± 0.98	28.80 ± 1.00	2.7555	2.749
17 (17,42)	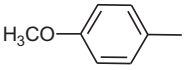	10.86 ± 1.40	32.60 ± 1.26**	2.5439	2.543
18 (18,43)	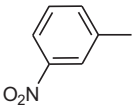	10.63 ± 1.14	31.07 ± 1.80	2.6074	2.61
19 (19,44)	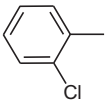	10.37 ± 1.02	28.59 ± 1.03	2.6848	2.68
20 (20,45)	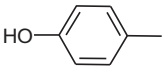	10.81 ± 1.61	30.11 ± 1.30	2.5891[a]	2.612[a]
23 (21,46)	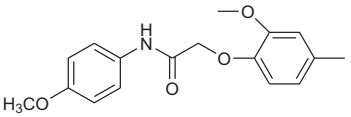	12.55 ± 1.03	36.98 ± 0.87**	2.7765	2.780
24 (22,47)	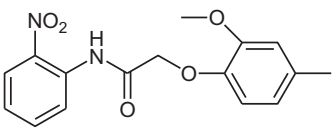	11.02 ± 1.28	33.80 ± 0.73**	2.8913	2.885

(*continued on next page*)

Table 1 (*continued*)

Cpd. no. (group no.)	R	Glucose uptake (mg/g/45 min)		CoMSIA	
		No insulin	With insulin	−ln MGU	Pred. act
25 (23,48)	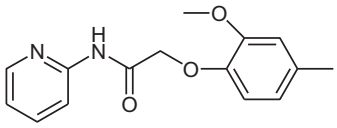	11.76 ± 1.54	33.28 ± 1.04**	2.8318	2.833
26 (24,49)	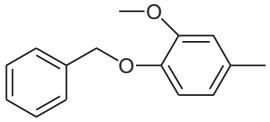	11.00 ± 0.91	31.61 ± 0.98*	2.8022	2.804
27 (25,50)	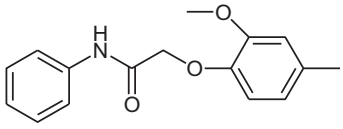	11.52 ± 1.54	34.55 ± 1.29**	2.7926[a]	2.713[a]
28 (26,51)	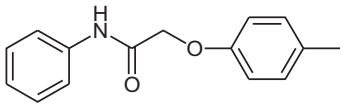	12.01 ± 1.08	33.88 ± 1.47**	2.7575	2.762
Std (27,52)	–	11.26 ± 0.85	36.60 ± 1.24**	–	–

Group 1: 7.80 ± 0.56, group 2: 25.56 ± 0.63.
Std: Standard drug (rosiglitazone).
[a] Test set compounds.
* $P < 0.05$.
** $P < 0.01$.

Table 2
Effect of glitazones on dexamethasone induced elevation of serum glucose and triglyceride levels.

Group	Treatment	Serum glucose (mg/dL)	Serum triglyceride (mg/dL)
1 (Normal)	Vehicle (10 mL/kg, p.o.)	118.8 ± 2.04**	92.67 ± 5.88**
2 (Positive control)	Dexamethasone (10 mg/kg, s.c.) + vehicle (10 mL/kg, p.o.)	238.0 ± 6.67**	270.0 ± 7.58**
3 (Standard drug)	Dexamethasone (10 mg/kg, s.c.) + rosiglitazone (10 mg/kg, p.o.)	147.8 ± 3.80**	177.5 ± 8.67**
4	Dexamethasone (10 mg/kg, s.c.) + compound **15** (10 mg/kg, p.o.)	209.8 ± 6.53*	242.3 ± 12.63*
5	Dexamethasone (10 mg/kg, s.c.) + compound **23** (10 mg/kg, p.o.)	132.3 ± 3.14**	184.5 ± 8.119**
6	Dexamethasone (10 mg/kg, s.c.) + compound **24** (10 mg/kg, p.o.)	171.7 ± 5.62**	194.5 ± 6.428**
7	Dexamethasone (10 mg/kg, s.c.) + compound **25** (10 mg/kg, p.o.)	185.2 ± 4.90**	186.5 ± 11.60**
8	Dexamethasone (10 mg/kg, s.c.) + compound **27** (10 mg/kg, p.o.)	177.3 ± 9.31**	193.0 ± 9.438**
9	Dexamethasone (10 mg/kg, s.c.) + compound **28** (10 mg/kg, p.o.)	222.3 ± 12.51	268.8 ± 12.73

Values mean ± SEM, $n = 6$.
s.c.: subcutaneously.
* $P < 0.05$.
** $P < 0.01$.

alone treated group. Compound **15** show good activity ($P < 0.05$). Compound **28** shows weak activity.

It is well known that insulin resistance in type II diabetes is not only associated with hyperglycemia but also with hyperlipidemia and atherosclerosis. Drugs that simultaneously ameliorate insulin resistance and hyperlipidemia, therefore, facilitates better management of type II diabetes [36,37]. The present study thus aims towards the development of such a drug. All the six compounds screened show both serum glucose and triglyceride lowering activity except compound **28**. Compounds **24** and **23** that emerge as the most active compounds in *in vitro* studies also show more or less similar trends in *in vivo* studies. Compounds **24**, **25** and **27** which are active in the *in vitro* study appear to be more or less same in the *in vivo* study as well. The results reveal some degree of correlation between serum glucose lowering activity and the serum triglyceride lowering activity in compounds **15**, **23**, **24**, **27**, **28** and rosiglitazone. Surprisingly, compound **28** (analogous to **27** and **23**) lacking vanillin as its trunk and methoxy group over the terminal aromatic ring (hydrophobic tail) fails to exhibit good activity.

3.3. Histopathology of the liver

PPAR ligand-induced hepato toxicity could be influenced by any number of mechanisms that may or may not be receptor-dependent. However, it is tempting to suggest that a specific PPAR ligand would cause toxicity solely through a receptor-mediated mechanism. This may not always be true and in any case not clearly understood. Liver, being an organ known to facilitate the first pass drug metabolism and detoxification process, thus gets itself damaged due to the release of toxic metabolites. Troglitazone was removed from the market after reports of some deaths because of the rare but severe hepatotoxicity. It also led to the discontinuation of ciglitazone and englitazone after the phase II clinical trials. Reported cases involving the newer TZDs, rosiglitazone and pioglitazone, have been fewer in number and less severe in consequence. Pharmacovigilance for hepatotoxicity is probably still required from the point of liver safety [38–40].

Eventhough there is a need for separate long term study on the liver toxicity of these compounds, we have made an attempt to

study the liver samples of the rats that received glitazones to study the effect of glitazones on dexamethasone induced elevation of serum glucose and triglyceride levels. After the sacrifice of animals, the rat liver samples from the selected groups of *in vivo* study subjected to the histopathological examination under light microscopy. The microscopic slides are shown in Table 3. Histopathological examinations of liver samples of vehicle treated group reveal no abnormalities (group 1, slides 1 and 2). Dexamethazone treated rat liver samples also show no abnormalities (group 2), possibly due to beneficial effect of dexamethazone as an anti-inflammatory agent at the dose of 10 mg/kg [41].

The standard drug, rosiglitazone, treated liver samples (group 3) were normal and no abnormalities were observed indicating that rosiglitazone reduces triglyceride levels to keep the liver cells almost normal [42].

Compound **23** treated rats (group 5) show vacuolar degeneration with focal necrobiotic changes (slide 10a), distortion of hepatocytes with multifocal infiltration of inflammatory cells (slide 10b) and cytoplasmic rarification of hepatocytes in liver parenchyma (slide 12). It also shows necrosis, severe infiltration of inflammatory cells and fibrous tissue proliferation at the periphery (slide 11). These observations indicate that compound **23** is prone to cause hepatotoxicity.

Rats that received compound **24** show no such severe abnormalities (group 6) in comparison to compound **23**. However, one of the animals shows eosinophilic degenerative area in liver parenchyma cells.

No sign of carcinoma, adenoma or preneoplastic lesion are observed in all the samples. These results are just preliminary and a separate long term toxicity study in the absence of dexamethazone is, however, required to bring in clarity with respect to toxicity profiles.

3.4. CoMSIA study

The 3D-QSAR models were derived employing the CoMSIA method with 20 compounds in the training set. The remaining four compounds, which are congeneric to training set compounds, constituted the test set. All the molecules were processed through the regular protocol of conformational analysis, energy minimization and denoting charges as described in Section 5. The alignment rule was optimized by using the appropriate common substructure, 2-(4-oxo-2-thioxothiazolidin-3-yl)-3-phenylpropanoic acid. The aligned training set is shown in Figs. 2–4. Field fit was used to optimize the alignment of molecules to a previously calculated steric, electrostatic, hydrophobicity, hydrogen bond donors and acceptors fields [43]. The PLS analyses on 20 training set compounds yielded a q^2 value (by LOO method) of 0.623 at the optimal number of components 4. The statistical data are shown in Table 4. Since the value of q^2 was reasonably good, no compound was removed as an outlier. Further, exclusion of compounds of a particular congeneric series may affect the predictivity of the model. The developed model show good predicted activities for the training set with low residual values as shown in Table 1 and Fig. 2. The predictive ability of the model was checked by predicting the activities of the test set compounds under different models. The model correlating the training set compounds with respect to steric, electrostatic, hydrophobic, hydrogen bond donor and hydrogen bond acceptor fields seems to be of better statistical significance when compared to all other models as shown in Table 4. The predicted activities of the training and test set compounds reported in this article are all from this optimized model.

Contour plots depicting the steric, electrostatic, hydrophobicity, hydrogen bond donor and hydrogen bond acceptor fields of the compounds generated based on the contributions towards the PLS model is shown in Fig. 2. Statistical parameters like q^2, r^2, F, P, steric and electrostatic contributions are given in Table 4. Steric, electrostatic, hydrophobicity, hydrogen bond donors and acceptors contributions were found to be 18.1%, 19.2%, 28.3%, 23.2% and 11.2%, respectively. The developed model was further validated by predicting the activities of the compounds of the test set.

3.5. Structure–activity relationship

The structure–activity relationships drawn from the above contour plots of the steric, electrostatic, hydrophobic, hydrogen bond acceptor and donor contributions of the generated CoMSIA model are, the superimposed common part of the structures, namely, polar rhodanine head followed by polar tyrosine or phenylalanine moiety at the third position and benzylidene moiety at the fifth position of the rhodanine ring seems to be the pharmacophore, as most of the compounds possesses this common substructure (Figs. 3–5). This indicates the necessity of relatively more polar acidic groups nearer the thiazolidine head.

The hydrophobic benzyloxy trunk, which in turn is connected to the two carbon acyl linker in association with the amide bond, also seems to be the important structural components for the compounds **23**–**28** to exhibit significant antidiabetic activity when compared to the rest of the compounds (Figs. 3–5). Regarding the hydrophobic trunk part, it appears vanillin is doing extremely good as many of the active compounds in the series contain the same. Compound **28** alone lacks the vanillin moiety from the series and fails to produce good activity. The two carbon acyl linker, in the form of amide bridge (CH_2CONH) in these compounds, appears to be an important requirement for their significant activity. The hydrophobic tail part which differs in most of the compounds is of major interest. Compound **23** with anisidine moiety is the most active compound from this series, even when compared with the standard drug (rosiglitazone). Compound **24** with *o*-nitro aniline as its tail also shows equally good activity.

The yellow contour over the phenylalanine or tyrosine part of the structure indicates that further extension is unfavorable for the glucose uptake activity (Fig. 3). Small blue contour for the electronegative groups near the acidic carboxyl group in Fig. 3 and orange contour for the hydrogen bond donor in the same region in Fig. 4, indicate that they will favor glucose uptake activity as evidenced by the yellow contour at the same region in Fig. 4 indicating, hydrogen bond acceptors which are the components of hydrogen bond donors at the similar positions are also essential for the activity.

An oxygen atom, connected directly to the aromatic ring (hydrophobic trunk) in the form of ether, is essential for the activity, as there is a blue contour near the red colored oxygen atoms in Fig. 3. A two carbon atom linker between the oxygen atom and terminal alicyclic or aromatic ring is ideal for the activity, as some of the compounds not containing the two carbon atom linker fail to show significant activity. Extension of carbon linker chain between the benzyl moiety and the terminal heterocyclic ring may pull the terminal ring towards the yellow region and decrease the activity. A prominent yellow contour in that region indicates that there should not be any substitution over those two carbon atoms.

In Fig. 4, the magenta colored contour after the benzoxy group (hydrophobic trunk) and over the two carbon linker indicates that introducing hydrogen bond donor in that region will reduce the activity. Compound **8** with phenolic OH group at the same position fails to produce good glucose uptake activity. However, compound **15** with a vanillin moiety as its trunk produces reasonably good glucose uptake activity. This could probably be due to the presence of OCH_3 group in vanillin structure apart from the hydrogen bond donor group (OH).

The cyan colored contours over the thiazolidine ring system, near the two carbon linker and after the hydrophobic tail, indicates

Table 3
Histopathological results of some liver samples.

Slide no.	Group no.	Treatment	Microscopic observations and pictures
1	1	Vehicle (10 mL/kg, p.o.)	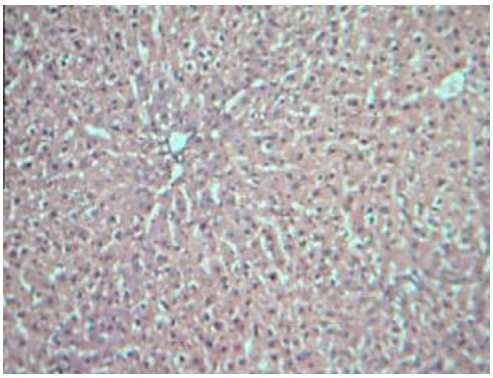 No abnormalities detected (H&E 45×)
2	1	-do-	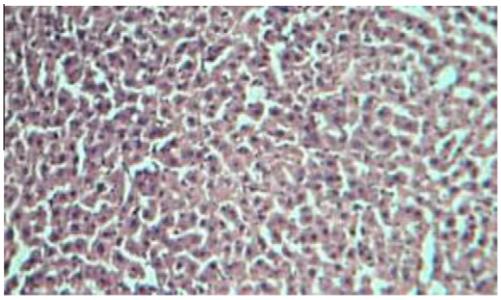 No abnormality detected (H&E 100×)
3	1	-do-	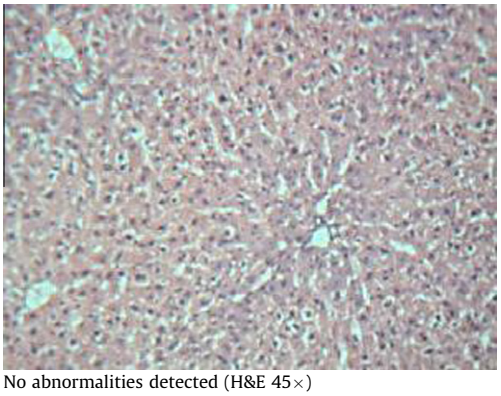 No abnormalities detected (H&E 45×)
4	2	Vehicle (10 mL/kg, p.o.) + dexamethasone (10 mg/kg, s.c.)	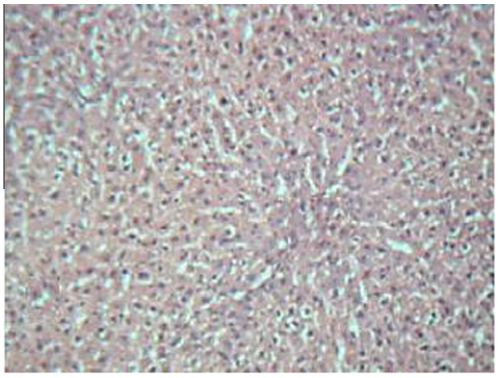 No abnormalities detected (H&E 45×)
5	2	-do-	

Table 3 (*continued*)

Slide no.	Group no.	Treatment	Microscopic observations and pictures
			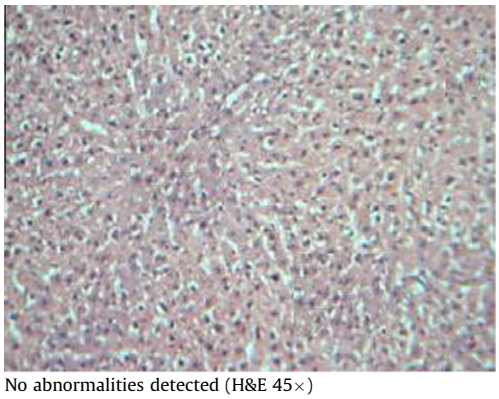
			No abnormalities detected (H&E 45×)
6	2	-do-	
7	3	Rosiglitazone (10 mg/kg, p.o.)	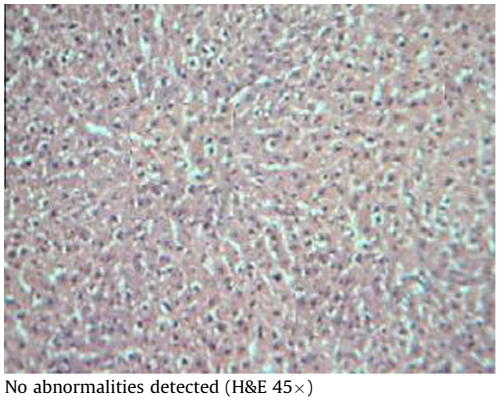
			No abnormalities detected (H&E 45×)
8	3	-do-	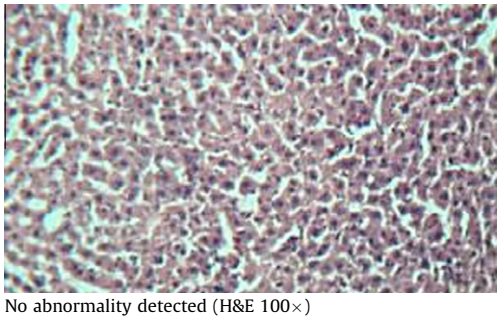
			No abnormality detected (H&E 100×)
9	3	-do-	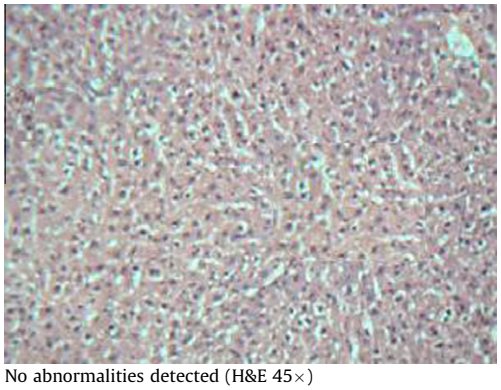
			No abnormalities detected (H&E 45×)

(*continued on next page*)

Table 3 (*continued*)

Slide no.	Group no.	Treatment	Microscopic observations and pictures
10a	5	Compound **23** (10 mg/kg, p.o.)	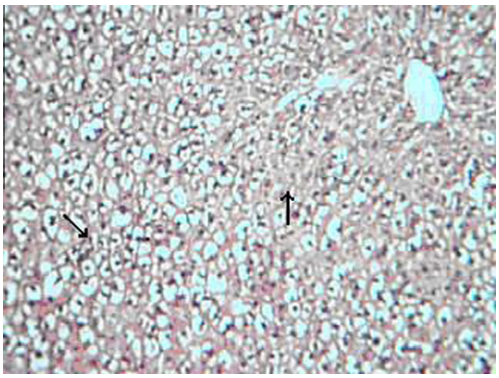 Note vacuolar degeneration with focal necrobiotic changes (H&E 100×)
10b	5	-do-	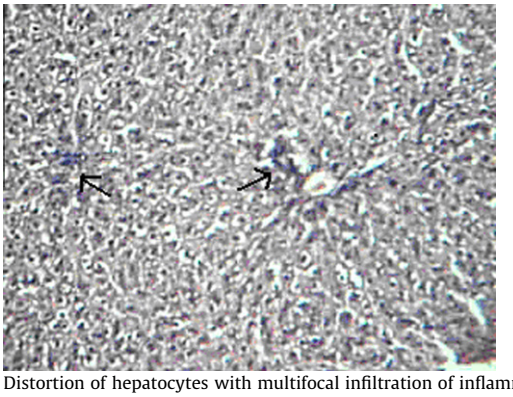 Distortion of hepatocytes with multifocal infiltration of inflammatory cells (H&E 100×)
11	5	-do-	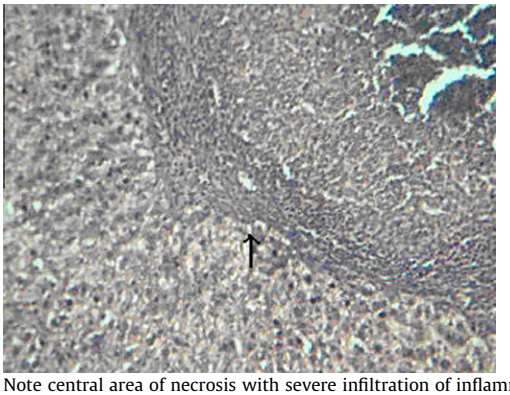 Note central area of necrosis with severe infiltration of inflammatory cells and fibrous tissue proliferation at the periphery (H&E 45×)
12	5	-do-	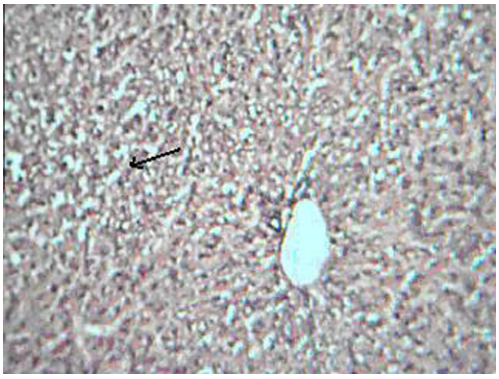 Cytoplasmic rarefication of hepatocytes in liver parenchyma (H&E 100×)

Table 3 (*continued*)

Slide no.	Group no.	Treatment	Microscopic observations and pictures
13	6	Compound **24** (10 mg/kg, p.o.)	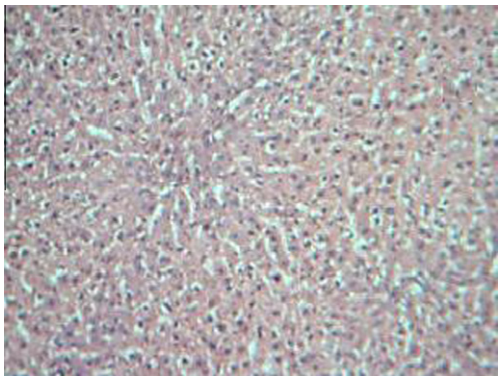 No abnormalities detected (H&E 45×)
14	6	-do-	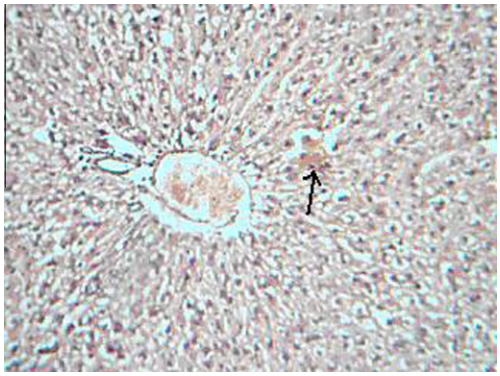 Note eosinophilic degenerative area in liver parenchyma (H&E 100×)
15	6	-do-	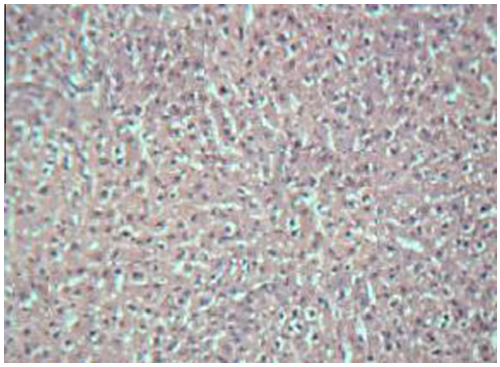 No abnormalities detected (H&E 45×)

NAD: No abnormality detected.

that introducing some hydrophobic groups at these positions will reduce the activity (Fig. 5). The small white contour near the benzoxy group (hydrophobic trunk) in Fig. 5 indicates that replacing OH group with OCH_3 group will enhance the activity (compounds **17** and **23**).

Finally, the developed CoMSIA model indicates that thiazolidinedione ring system with tyrosine substitution at the third position and a hydrophobic trunk connected to the hydrophobic tail via a two carbon linker at the fifth position is essential for these to exhibit significant activity.

4. Summary and conclusion

In summary, we report here a simple, efficient method to synthesize some novel rhodanines incorporated with amino acids such as phenylalanine and tyrosine. We have thus found a new series of glitazones with different body make up having promising levels of glucose uptake activity, glucose lowering activity and triglyceride lowering activity. Compounds **23** and **24** seem to be the candidate compounds to investigate further for their efficacy and safety.

5. Experimental section

5.1. Chemistry

The melting points were determined in open capillaries using Veego VMP-1 melting point apparatus and are uncorrected. The temperatures were expressed in °C. The IR spectra were recorded on Shimadzu infrared-283 FTIR spectrometer by KBr pellet technique and are expressed in cm^{-1}. NMR spectra were recorded on a Bruker Avance 500 and 400 spectrometers with TMS as internal standard (500 and 400 MHz for ^1H NMR, 125 and 100 MHz for ^{13}C) and DMSO-d_6 as solvent. The chemical shifts are expressed in δ ppm and the following abbreviations are used; s = singlet,

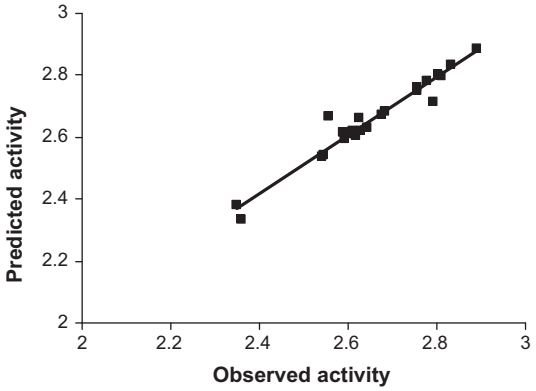

Fig. 2. Correlation between the observed and predicted activities of the developed CoMSIA model: ■ indicates the training set compounds and ● indicates the test set compounds.

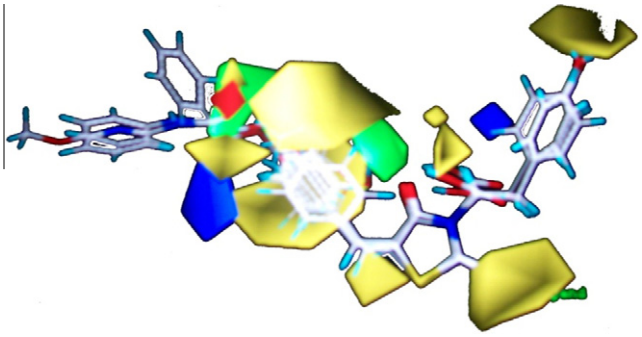

Fig. 3. Aligned glitazones CoMSIA SD *x* coefficient contour plot: Green contours indicate regions where steric bulk is favorable and yellow contours indicate regions where steric bulk is not favored; Blue contours indicate regions where electronegative groups increase activity and red contours indicate regions where electronegative groups decrease activity. (For interpretation of the references to color in this figure legend, the reader is referred to the web version of this article.)

bs = broad singlet, d = doublet, bd = broad doublet, t = triplet, bt = broad triplet, q = quartlet, m = multiplet, bm = broad multiplet. Attempt has also been made to identify the peaks in ^{13}C NMR spectra based on the relative chemical environments of the carbon atoms in the structure. Mass spectra were recorded using high resolution mass spectrometer (HRMS) and liquid chromatography mass spectrometer (LCMS) under electro spray ionization technique, using time of flight and triple quadrupole mass analyzers, respectively. All the compounds synthesized showed ^{1}H and ^{13}C NMR, IR and Mass spectra consistent with the proposed structures. Column chromatography was done with Merck silica gel 60 (0.0634, 200 mm). When reactions were performed in anhydrous conditions, the mixtures were maintained under nitrogen. TLC was performed using 4% methanol in chloroform as mobile phase on aluminum plates which are precoated with silica gel GF, unless otherwise stated. Compounds were named following the IUPAC rules.

*5.1.1. General procedure followed for the preparation of **3** and **4***

Water (10 mL) and ammonia solution (30 mL, 25–30%) were transferred into a conical flask. The conical flask was placed in ice bath and the temperature was maintained at 0–5 °C. Carbon disulfide (0.0031 M) was then added. (±)-Tyrosine or (±)-phenylalanine (0.003 M) was added slowly to this solution for a period of 30 min with continuous stirring. Cotton plug was put to the flask and the reaction mixture was continued to stir for 10 h and

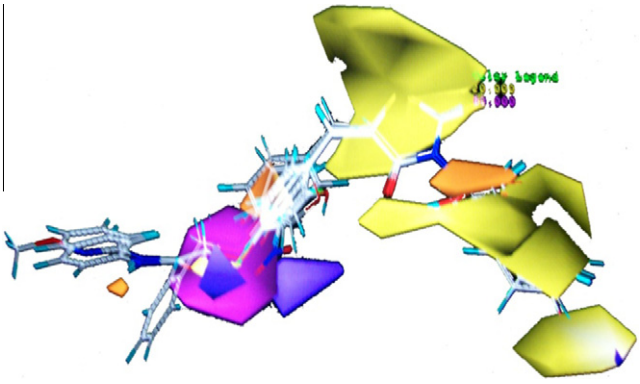

Fig. 4. Aligned glitazones CoMSIA SD *x* coefficient contour plot: Orange contours indicate regions where hydrogen bond donor is favorable and magenta contours indicate regions where hydrogen bond donor is not favored; yellow contours indicate regions where hydrogen bond acceptors increase activity and purple contours indicate regions where hydrogen bond acceptors decrease activity. (For interpretation of the references to color in this figure legend, the reader is referred to the web version of this article.)

allowed to stand for 2 h in a refrigerator to yield dithiocarbamate of the corresponding amino acid (**1** and **2**). Sodium chloroacetate solution was prepared, by dissolving chloroacetic acid (0.003 M) and NaOH (0.003 M) each in 3 mL of water, separately. Both were then mixed and stirred for 30 min. Solid sodium carbonate was then added slowly until the reaction mixture became basic to litmus. Sodium chloroacetate solution was added to a flask containing dithiocarbamate solution slowly at 5–10 °C under stirring. The reaction mixture was allowed to stir for 1 h. The uncyclized *N*-substituted rhodanine formed was cyclized by adding 10 mL of 6 N HCl, 2 or 3 drops of phosphorous oxychloride and heated at 60–70 °C for about 3 h. The reaction was monitored through TLC using 20% methanol in chloroform as the mobile phase. The spots on TLC were detected using alcoholic *dodeca*-phosphomolybdinum staining and heating, apart from using Ninhydrin reagent. The reaction mixture was allowed to cool. The solid formed was filtered and recrystallised with diethyl ether to obtain **3** and **4**. Compounds **5–12** and **13–20** were prepared by subjecting **3** and **4** to the Knoevenagel condensation reaction with different substituted aldehydes.

*5.1.1.1. (±)-2-(4-Oxo-2-thioxothiazolidin-3-yl)-3-phenylpropanoic acid (**3**).* Pale yellow amorphous solid, mp 188–190 °C, Yield 86%. FTIR (KBr, cm^{-1}): 3400–2700 (O–H), 3028 (Ar–H), 2924 (AliC–H), 1741 (C=O), 1708 (C=O), 1494 (ArC=C), 1222 (C=S), 1201 (C–O), 1174 (C–N). ^{1}H NMR (300 MHz, DMSO-d_6, δ ppm): 3.54 (t, J = 6.0 Hz, 2H, CH_2), 3.82 (s, 2H, CH_2), 5.74 (bm, 1H, α-hydrogen, CH), 7.14–7.40 (m, 5H, ArH). ^{13}C NMR (500 MHz, DMSO-d_6, δ ppm): 33.41 (CH_2), 35.16 (CH_2), 58.51 (CH), 127.12 (=C), 128.73 (2ArC), 129.51 (2ArC), 137.16 (1ArC), 169.33 (C=O), 174.43 (C=O), 203.11 (C=S). HRMS (ES-TOF) *m*/*z* found 304.0068 (M+Na), calculated 304.0078 (M+Na).

*5.1.1.2. (±)-2-((Z)-5-benzylidene-4-oxo-2-thioxothiazolidin-3-yl)-3-(4-hydroxyphenyl)propanoic acid (**4**).* Yellow crystals, mp 210–212 °C, Yield 58%. FTIR (KBr, cm^{-1}): 3500–2900 (O–H), 3022 (Ar–H), 2960 (AliC–H), 1707 (C=O), 1608 (C=O), 1512 (ArC=C), 1267 (C=S), 1244 (C–O), 1153 (C–N). ^{1}H NMR (400 MHz, DMSO-d_6, δ ppm): 3.37 (bt, 2H, CH_2), 5.43 (bm, 1H, CH), 6.55 (d, J = 8.5 Hz, 2H, ArH), 6.85 (d, J = 8.5 Hz, 2H, ArH), 7.45–7.62 (m, 5H, ArH), 7.64 (s, 1H, =CH), 8.91 (bs, 1H, OH). ^{13}C NMR (400 MHz, DMSO-d_6, δ ppm): 34.08 (CH_2), 61.22 (CH), 115.57 (1ArC), 115.79 (2ArC), 125.70 (=C), 129.71 (1ArC), 130.02 (1ArC), 130.33 (1ArC), 130.39 (1ArC), 130.69 (2ArC), 130.91 (1ArH),

Table 4
PLS statistics of the CoMSIA models.

PLS statistics parameters	CoMSIA							
	SE	SHE	SED	SEA	SEDA	SEHD	SEHA	SEHDA
q^2	0.520	0.558	0.527	0.540	0.545	0.585	0.609	0.623
r^2	0.798	0.873	0.806	0.855	0.857	0.928	0.942	0.989
SEE	0.163	0.122	0.117	0.089	0.078	0.041	0.036	0.018
F	105.76	119.40	124.29	137.60	141.55	170.25	182.86	193.99
PLS components	4	4	4	4	4	4	4	4
P value	0	0	0	0	0	0	0	0
Steric	0.479	0.285	0.246	0.359	0.212	0.145	0.203	0.181
Electrostatic	0.521	0.314	0.455	0.491	0.325	0.272	0.279	0.192
Hydrophobic	–	0.401	–	–	–	0.358	0.382	0.283
H donor	–	–	0.299	–	0.303	0.225	–	0.232
H acceptor	–	–	–	0.150	0.160	–	0.136	0.112
Pred r^2 for test set	0.385	0.435	0.397	0.470	0.487	0.528	0.553	0.570

SEE = Standard error of estimate, S = steric field, E = electrostatic field, H = hydrophobic field, D = hydrogen bond donor, A = hydrogen bond acceptor.

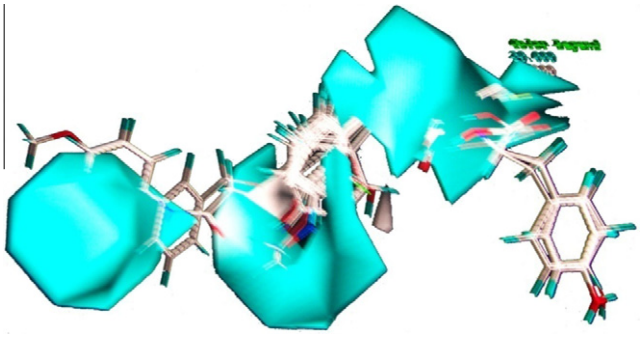

Fig. 5. Aligned glitazones CoMSIA SD *x* coefficient contour plot: Cyan contours indicate regions where hydrophobicity is unfavorable and white contours indicate regions where hydrophobicity favored. (For interpretation of the references to color in this figure legend, the reader is referred to the web version of this article.)

131.02 (1ArC), 131.29 (1ArH), 156.98 (=CH), 170.82 (C=O), 171.42 (C=O), 190.77 (C=S). HRMS (ES-TOF) *m*/*z* found 408.0345 (M+Na), calculated 408.1046 (M+Na).

5.1.2. General procedure for the Knoevenagel condensation reaction

Equimolar amounts of the substrate, **3** or **4**, **22** (0.002 M) and 20–30 mL of dry toluene, were transferred to a flask. *N*-methyl piperazine (0.0001 M), ammonium acetate (0.0001 M) and molecular sieves (0.5 g) were then added. The reaction mixture was stirred for 5 min and then heated under reflux at 110 °C with occasional stirring for about 15 h. After the completion of the reaction, the reaction mixture was allowed to cool and the precipitated solid was filtered and recrystallized using methanol to obtain the pure compound [24].

*5.1.2.1. (±)-2-((Z)-5-(4-chlorobenzylidene)-4-oxo-2-thioxothiazolidin-3-yl)-3-phenylpropanoic acid (**5**).* Yellow crystals, mp 250–252 °C, Yield 76%. FTIR (KBr, cm^{-1}): 3400 (O–H), 3014 (Ar–H), 2943 (AliC–H), 1705 (C=O), 1641 (C=O), 1585 (ArC=C), 1274 (C=S), 1238 (C–O), 1166 (C–N), 675 (C–Cl). ^{1}H NMR (400 MHz, DMSO-d_6, δ ppm): 3.53 (bt, 2H, CH_2), 5.50 (bm, 1H, CH), 7.07–7.62 (m, 9H, ArH), 7.70 (s, 1H, =CH). ^{13}C NMR (400 MHz, DMSO-d_6, δ ppm): 34.19 (CH_2), 61.69 (CH), 122.30 (=C), 126.05 (2ArC), 128.09 (2ArC), 128.59 (2ArC), 129.47 (1ArC), 130.72 (1ArC), 131.83 (1ArC), 132.12 (2ArC), 135.39 (1ArC), 135.77 (=CH), 166.75 (C=O), 168.82 (C=O), 193.33 (C=S). HRMS (ES-TOF) *m*/*z* found 426.0004 (M+Na), calculated 426.0001 (M+Na).

*5.1.2.2. (±)-2-((Z)-5-(4-(dimethylamino)benzylidene)-4-oxo-2-thioxothiazolidin-3-yl)-3-phenylpropanoic acid (**6**).* Orange red crystals, mp 282–286 °C, Yield 75%. FTIR (KBr, cm^{-1}): 3350–2500 (O–H), 3028 (Ar–H), 2945 (AliC–H), 1701 (C=O), 1673 (C=O), 1525 (ArC=C), 1280 (C=S), 1226 (O–H), 1172 (C–N). ^{1}H NMR (400 MHz, DMSO-d_6, δ ppm): 3.50 (bt, 2H, CH_2), 3.04 (s, 6H, 2 × CH_3), 5.50 (bm, 1H, CH), 6.82 (d, *J* = 9.04 Hz, 2H, ArH), 7.05–7.18 (m, 5H, ArH), 7.40 (d, *J* = 9.04 Hz, 2H, ArH), 7.53 (s, 1H, =CH). HRMS (ES-TOF) *m*/*z* found 435.0803 (M+Na), calculated 435.1007 (M+Na).

*5.1.2.3. (±)-2-((Z)-5-benzylidene-4-oxo-2-thioxothiazolidin-3-yl)-3-phenylpropanoic acid (**7**).* Pale yellow crystals, mp 236–239 °C, Yield 78%. FTIR (KBr, cm^{-1}): 3000–2500 (O–H), 3005 (Ar–H), 2939 (AliC–H), 1697 (C=O), 1593 (ArC=C), 1271 (C=S), 1232 (C–O), 1172 (C–N). ^{1}H NMR (400 MHz, DMSO-d_6, δ ppm): 3.54 (bt, 2H, CH_2), 5.49 (bm, 1H, CH), 7.07–7.20 (m, 5H, ArH), 7.50–7.60 (m, 5H, ArH), 7.69 (s, 1H, =CH). ^{13}C NMR (400 MHz, DMSO-d_6, δ ppm): 34.32 (CH_2), 61.99 (CH), 121.68 (=C), 125.96 (2ArC), 128.06 (2ArC), 128.56 (2ArC), 129.41 (1ArC), 130.48 (2ArC), 130.71 (1ArC), 131.91 (1ArC), 132.97 (1ArC), 139.04 (=CH), 166.88 (C=O), 168.67 (C=O), 194 (C=S). HRMS (ES-TOF) *m*/*z* found 392.0402 (M+Na), calculated 392.0391 (M+Na).

*5.1.2.4. (±)-2-((Z)-5-(4-hydroxybenzylidene)-4-oxo-2-thioxothiazolidin-3-yl)-3-phenylpropanoic acid (**8**).* Yellow amorphous solid, mp 297–300 °C, Yield 73%. FTIR (KBr, cm^{-1}): 3250–2500 (O–H), 3005 (Ar–H), 2943 (AliC–H), 1695 (C=O), 1633 (C=O), 1579 (ArC=C), 1267 (C=S), 1219 (C–O), 1168 (C–N). ^{1}H NMR (400 MHz, DMSO-d_6, δ ppm): 3.52 (bt, 2H, CH_2), 5.53 (bm, 1H, CH), 6.90 (d, *J* = 8.72 Hz, 2H, ArH), 7.05–7.18 (m, 5H, ArH), 7.42 (d, *J* = 8.68 Hz, 2H, ArH), 7.55 (s, 1H, =CH), 9.76 (bs, 1H, OH). ^{13}C NMR (400 MHz, DMSO-d_6, δ ppm): 34.35 (CH_2), 61.63 (CH), 116.71 (2ArC), 123.55 (=C), 125.96 (1ArC), 128.03 (2ArC), 128.61 (2ArC), 128.83 (1ArC), 132.80 (1ArC), 133.05 (2ArH), 133.98 (=CH), 161.16 (1ArC), 167.03 (C=O), 169.34 (C=O), 193.63 (C=S). HRMS (ES-TOF) *m*/*z* found 408.0344 (M+Na), calculated 408.0340 (M+Na).

*5.1.2.5. (±)-2-((Z)-5-(4-methoxybenzylidene)-4-oxo-2-thioxothiazolidin-3-yl)-3-phenylpropanoic acid (**9**).* Yellow crystlas, mp 264–267 °C, Yield 81%. FTIR (KBr, cm^{-1}): 3100–2500 (O–H), 3005 (Ar–H), 2941 (AliC–H), 1687 (C=O), 1635 (C=O), 1583 (ArC=C), 1265 (C=S), 1220 (C–O), 1170 (C–N). ^{1}H NMR (400 MHz, DMSO-d_6, δ ppm): 3.52 (bt, 2H, CH_2), 3.82 (s, 3H, CH_3), 5.50 (bm, 1H, CH), 7.05–7.20 (m, 7H, ArH), 7.47 (s, 1H, =CH), 7.55 (d, *J* = 8.8 Hz, 2H, ArH). ^{13}C NMR (400 MHz, DMSO-d_6, δ ppm): 34.31 (CH_2), 55.51 (CH_3), 61.86 (CH), 115.07 (2ArC), 125.57 (=C), 125.93 (2ArC), 128.03 (2ArC), 128.56 (2ArC), 130.12 (1ArC), 132.01 (1ArC), 132.69 (2ArH), 133.09 (=CH), 161.29 (C=O), 168.62

(C=O), 194.27 (C=S). HRMS (ES-TOF) *m*/*z* found 422.0498 (M+Na), calculated 422.0961 (M+Na).

*5.1.2.6. (±)-2-((Z)-5-((furan-2-yl)methylidene)-4-oxo-2-thioxothiazolidin-3-yl)-3-phenylpropanoic acid (**10**).* Black crystals, mp 221–224 °C, Yield 64%. FTIR (KBr, cm^{-1}): 3450–2700 (O–H), 3000 (Ar–H), 2949 (AliC–H), 1705 (C=O), 1668 (C=O), 1556 (ArC=C), 1239 (C=S), 1211 (C–O), 1082 (C–N). ^{1}H NMR (400 MHz, DMSO-d_6, δ ppm): 3.50 (bt, 2H, CH_2), 5.58 (bm, 1H, CH), 7.18–7.78 (m, 8H, ArH) 7.70 (s, 1H, =CH). ^{13}C NMR (400 MHz, DMSO-d_6, δ ppm): 34.33 (CH_2), 61.75 (CH), 121.41 (=C), 128.87 (2ArC), 129.48 (1ArC), 129.67 (2ArC), 137.24 (1ArC), 138.35 (1ArC), 133.05 (=CH), 139.78 (1ArC), 143.2 (1ArC), 148.0 (1ArC), 169.37 (C=O), 174.39 (C=O), 198.76 (C=S). HRMS (ES-TOF) *m*/*z* found 382.118 (M+Na), calculated 382.2016 (M+Na).

*5.1.2.7. (±)-2-((Z)-5-(2-hydroxybenzylidene)-4-oxo-2-thioxothiazolidin-3-yl)-3-phenylpropanoic acid (**11**).* Yellow crystals, mp 272–275 °C, Yield 62%. FTIR (KBr, cm^{-1}): 3460–3050 (O–H), 3042 (Ar–H), 2965 (AliC–H), 1701 (C=O), 1677 (C=O), 1589 (ArC=C), 1228 (C=S), 1228 (C–O), 1155 (C–N). ^{1}H NMR (400 MHz, DMSO-d_6, δ ppm): 3.52 (bt, 2H, CH_2), 5.50 (bm, 1H, CH), 7.08–7.58 (m, 9H, ArH), 7.71 (s, 1H, =CH), 9.62 (bs, 1H, OH). HRMS (ES-TOF) *m*/*z* found 408.2018 (M+Na), calculated 408.3009 (M+Na).

*5.1.2.8. (±)-2-((Z)-5-(2,4-dichlorobenzylidene)-4-oxo-2-thioxothiazolidin-3-yl)-3-phenylpropanoic acid (**12**).* Light yellow crystals, mp 201–204 °C, Yield 64%. FTIR (KBr, cm^{-1}): 3300–2600 (O–H), 3026 (Ar–H), 2951 (AliC–H), 1718 (C=O), 1676 (C=O), 1560 (ArC=C), 1274 (C=S), 1201 (C–O), 1155 (C–N), 653 (C–Cl). ^{1}H NMR (400 MHz, DMSO-d_6, δ ppm): 3.55 (bt, 2H, CH_2), 5.50 (bm, 1H, CH), 7.08–7.60 (m, 7H, ArH), 7.68 (s, 1H, ArH), 7.73 (s, 1H, =CH). HRMS (ES-TOF) *m*/*z* found 461.2013 (M+Na), calculated 461.1820 (M+Na).

*5.1.2.9. (±)-2-((Z)-5-benzylidene-4-oxo-2-thioxothiazolidin-3-yl)-3-(4-hydroxyphenyl)propanoic acid (**13**).* Yellow crystals, mp 210–212 °C, Yield 58%. FTIR (KBr, cm^{-1}): 3500–2900 (O–H), 3022 (Ar–H), 2960 (AliC–H), 1707 (C=O), 1608 (C=O), 1512 (ArC=C), 1267 (C=S), 1244 (C–O), 1153 (C–N). ^{1}H NMR (400 MHz, DMSO-d_6, δ ppm): 3.37 (bt, 2H, CH_2), 5.43 (bm, 1H, CH), 6.55 (d, *J* = 8.5 Hz, 2H, ArH), 6.85 (d, *J* = 8.5 Hz, 2H, ArH), 7.45–7.62 (m, 5H, ArH), 7.64 (s, 1H, =CH), 8.91 (bs, 1H, OH). ^{13}C NMR (400 MHz, DMSO-d_6, δ ppm): 34.08 (CH_2), 61.22 (CH), 115.57 (1ArC), 115.79 (2ArC), 125.70 (=C), 129.71 (1ArC), 130.02 (1ArC), 130.33 (1ArC), 130.39 (1ArC), 130.69 (2ArC), 130.91 (1ArH), 131.02 (1ArC), 131.29 (1ArH), 134.98 (=CH), 170.82 (C=O), 171.42 (C=O), 190.77 (C=S). HRMS (ES-TOF) *m*/*z* found 408.0345 (M+Na), calculated 408.0841 (M+Na).

*5.1.2.10. (±)-2-((Z)-5-(4-chlorobenzylidene)-4-oxo-2-thioxothiazolidin-3-yl)-3-(4-hydroxyphenyl)propanoic acid (**14**).* Cream colored crystals, mp 237–240 °C, Yield 65%. FTIR (KBr, cm^{-1}): 3500–2800 (O–H), 3024 (Ar–H), 2906 (AliC–H), 1707 (C=O), 1637 (C=O), 1521 (ArC=C), 1300 (C=S), 1210 (C–O), 1099 (C–N), 534 (C–Cl). ^{1}H NMR (400 MHz, DMSO-d_6, δ ppm): 3.40 (bt, 2H, CH_2), 5.40 (bm, 1H, CH), 6.60 (d, *J* = 8.3 Hz, 2H, ArH), 6.85 (d, *J* = 8.3 Hz, 2H, ArH), 7.57–7.63 (m, 4H, ArH), 7.68 (s, 1H, =CH), 7.93 (bs, 1H, OH). HRMS (ES-TOF) *m*/*z* found 442.0615 (M+Na), calculated 442.1075 (M+Na).

*5.1.2.11. (±)-2-((Z)-5-(4-hydroxy-3-methoxybenzylidene)-4-oxo-2-thioxothiazolidin-3-yl)-3-(4-hydroxyphenyl)propanoic acid (**15**).* Orange crystals, mp 282–286 °C, Yield 76%. FTIR (KBr, cm^{-1}): 3400–2500 (O–H), 3039 (Ar–H), 2929 (AliC–H), 1701 (C=O), 1637 (C=O), 1512 (ArC=C), 1244 (C=S), 1176 (O–H), 1041 (C–N). ^{1}H NMR (500 MHz, DMSO-d_6, δ ppm): 3.40 (bt, 2H, CH_2), 3.83 (s, 3H, CH_3), 5.56 (bm, 1H, CH), 6.50–7.0 (m, 7H, ArH), 7.64 (s, 1H, =CH), 9.14 (bs, 1H, OH), 9.21 (bs, 1H, OH). LCMS (LC-MSD-Trap-SL) *m*/*z* found 432.0 (M+1), calculated 432.0 (M+1).

*5.1.2.12. (±)-2-((Z)-5-(2,4-dichlorobenzylidene)-4-oxo-2-thioxothiazolidin-3-yl)-3-(4-hydroxyphenyl)propanoic acid (**16**).* Yellow amorphous solid, mp > 300 °C, Yield 59%. FTIR (KBr, cm^{-1}): 3400–2500 (O–H), 3022 (Ar–H), 2960 (AliC–H), 1716 (C=O), 1683 (C=O), 1512 (ArC=C), 1244 (C=S), 1215 (C–O), 1111(C–N), 574 (C–Cl). ^{1}H NMR (500 MHz, DMSO-d_6, δ ppm): 3.38 (bt, 2H, CH_2), 5.75 (bm, 1H, CH), 6.52–7.6 (m, 7H, ArH), 7.85 (s, 1H, =CH), 9.25 (bs, 1H, OH). LCMS (LC-MSD-Trap-SL) *m*/*z* found 454.0 (M+1), calculated 454.0 (M+1).

*5.1.2.13. (±)-2-((Z)-5-(4-methoxybenzylidene)-4-oxo-2-thioxothiazolidin-3-yl)-3-(4-hydroxyphenyl)propanoic acid (**17**).* Yellow crystals, mp 223–225 °C, Yield 61%. FTIR (KBr, cm^{-1}): 3500–2500 (O–H), 3026 (Ar–H), 2960 (AliC–H), 1732 (C=O), 1707 (C=O), 1589 (ArC=C), 1230 (C=S), 1170 (C–O), 1012 (C–N). ^{1}H NMR (500 MHz, DMSO-d_6, δ ppm): 3.40 (t, 2H, CH_2), 3.88 (s, 3H, CH_3), 5.62 (bm, 1H, CH), 6.65 (d, *J* = 8.4 Hz, 2H, ArH), 6.70 (d, *J* = 8.5, 2H, ArH), 6.94 (d, *J* = 8.4 Hz, 2H, ArH), 7.03 (d, *J* = 8.5 Hz, 2H, ArH), 7.84 (s, 1H, =CH), 9.28 (bs, 1H, OH), 10.34 (bs, 1H, OH). ^{13}C NMR (500 MHz, DMSO-d_6, δ ppm): 36.00 (CH_2), 56.07 (CH_3), 59.13 (CH), 115.35 (2ArC), 115.51 (2ArC), 125.93 (=C), 130.22 (1ArC), 130.77 (2ArC), 130.90 (2ArC), 133.47 (=CH), 156.22 (1ArC), 156.92 (1ArC), 157.64 (1ArC), 170.90 (C=O), 175.78 (C=O), 196.0 (C=S). LCMS (LC-MSD-Trap-SL) *m*/*z* found 416.8 (M+1), calculated 415.0 (M+1).

*5.1.2.14. (±)-2-((Z)-5-(3-nitrobenzylidene)-4-oxo-2-thioxothiazolidin-3-yl)-3-(4-hydroxyphenyl)propanoic acid (**18**).* Pale yellow crystals, mp 260–262 °C, Yield 59%. FTIR (KBr, cm^{-1}): 3500–2500 (O–H), 3022 (Ar–H), 2929 (AliC–H), 1705 (C=O), 1700 (C=O), 1512 (ArC=C), 1244 (C=S), 1174 (C–O), 1014 (C–N). ^{1}H NMR (500 MHz, DMSO-d_6, δ ppm): 3.40 (bt, 2H, CH_2), 5.75 (bm, 1H, CH), 6.80–8.50 (m, 8H, ArH), 7.97 (s, 1H, =CH), 9.20 (bs, 1H, OH). ^{13}C NMR (500 MHz, DMSO-d_6, δ ppm): 32.75 (CH_2), 59.38 (CH), 115.41 (1ArC), 115.61 (2ArC), 122.39 (=C), 125.79 (1ArC), 127.02 (1ArC), 128.07 (1ArC), 130.33 (2ArC), 130.88 (1ArC), 131.52 (1ArC), 134.73 (=CH), 148.80 (1ArC), 156.21 (1ArC), 169.09 (C=O), 172.79 (C=O), 188 (C=S). LCMS (LC-MSD-Trap-SL) *m*/*z* found 431.5 (M+1), calculated 431.0 (M+1).

*5.1.2.15. (±)-2-((Z)-5-(2-chlorobenzylidene)-4-oxo-2-thioxothiazolidin-3-yl)-3-(4-hydroxyphenyl)propanoic acid (**19**).* Brown crystals, mp 229–231 °C, Yield 55%. FTIR (KBr, cm^{-1}): 3500–2500 (O–H), 3039 (Ar–H), 2960 (AliC–H), 1728 (C=O), 1700 (C=O), 1514 (ArC=C), 1244 (C=S), 1091 (C–O), 1041 (C–N), 574 (C–Cl). ^{1}H NMR (500 MHz, DMSO-d_6, δ ppm): 3.40 (bt, 2H, CH_2), 5.73 (bm, 1H, CH), 6.60–7.60 (m, 8H, ArH), 7.90 (s, 1H, =CH), 9.28 (bs, 1H, OH). LCMS (LC-MSD-Trap-SL) *m*/*z* found 420.0 (M+1), calculated 420.0 (M+1).

*5.1.2.16. (±)-2-((Z)-5-(4-hydroxybenzylidene)-4-oxo-2-thioxothiazolidin-3-yl)-3-(4-hydroxyphenyl)propanoic acid (**20**).* Yellow crystals, mp 278–281 °C, Yield 61%. FTIR (KBr, cm^{-1}): 3500–2500 (O–H), 3022 (Ar–H), 2960 (AliC–H), 1700 (C=O), 1707 (C=O), 1512 (ArC=C), 1244 (C=S), 1176 (C–O), 1041 (C–N). ^{1}H NMR (500 MHz, DMSO-d_6, δ ppm): 3.40 (bt, 2H, CH_2), 5.64 (bm, 1H, CH), 6.50 (d, *J* = 8.5 Hz, 2H, ArH), 6.85 (d, *J* = 8.5, 2H, ArH), 6.95 (d, *J* = 8.5 Hz, 2H, ArH), 7.45 (d, *J* = 8.5 Hz, 2H, ArH), 7.69 (s, 1H, =CH), 9.15 (bs, 1H, OH), 9.20 (bs, 1H, OH). LCMS (LC-MSD-Trap-SL) *m*/*z* found 400.0 (M−1), calculated 400.0 (M−1).

*5.1.3. Procedure for the preparation of compounds **23–28***

Alicyclic or aromatic amine (0.1 M) and triethylamine (0.1 M) along with dry chloroform (80 mL) were transferred into a flask fitted with a guard tube. The mixture was allowed to stir under ice cold conditions (0–5 °C). Chloroacetyl chloride (0.11 M) was added drop wise for a period of 30 min. The reaction mixture was continued to stir to reach room temperature. The reaction mixture was again stirred for about 6 h at 30–35 °C. The reaction was monitored through TLC using 20% ethyl acetate in pet ether as a mobile phase. After the completion of the reaction, the solvent was evaporated. The product obtained was washed with water and dried to obtain the acylated amines **21** (90–99%).

A mixture of acylated amine **21** (0.09 M), finely powdered anhydrous K_2CO_3 (0.125 M) and vanillin (0.12 M) along with 80 mL of dry acetone was stirred at 35–40 °C for about 36 h. The progress of the reaction was monitored by TLC using 15% ethyl acetate in pet ether as a mobile phase. The reaction mixture was then poured into water and extracted with ethyl acetate. The ethyl acetate layer was washed thrice with 10% aqueous NaOH solution, washed once with brine solution and then finally dried over anhydrous Na_2SO_4. The ethyl acetate layer was evaporated to obtain compound **22** (65–80%). Compounds **23**–**28** were prepared by subjecting the substituted aldehyde **22** to the Knoevenagel condensation reaction with tyrosine incorporated rhodanine **4**.

*5.1.3.1. (±)-2-((Z)-5-(4-((4-methoxyphenylcarbamoyl)methoxy)-3-methoxybenzylidene)-4-oxo-2-thioxo-thiazolidin-3-yl)-3-(4-hydroxyphenyl)propanoic acid (**23**).* Yellow crystals, 262–265 °C, Yield 62%. FTIR (KBr, cm^{-1}): 3500–2500 (O–H), 3205 (N–H), 3043 (Ar–H), 2933 (AliC–H), 1693 (C=O), 1662 (C=O), 1508 (ArC=C), 1284 (C=S), 1234 (C–O), 1145 (C–N). ^{1}H NMR (500 MHz, DMSO-d_6, δ ppm): 3.40 (bt, 2H, CH_2), 3.72 (s, 3H, CH_3), 3.87 (s, 3H, CH_3), 4.82 (s, 2H, CH_2), 5.65 (bm, 1H, CH), 6.60–7.60 (m, 11H, ArH), 7.53 (s, 1H, =CH), 9.10 (bs, 1H, OH), 9.85 (s, 1H, NH), 10.08 (s, 1H, OH). ^{13}C NMR (500 MHz, DMSO-d_6, δ ppm): 55.65 (2 × CH_3), 56.12 (CH_2), 56.50 (CH), 68.21 (CH_2), 110.63 (=C), 113.31 (1ArC), 114.39 (4ArC), 115.37 (1ArC), 115.50 (2ArC), 121.49 (4ArC), 130.76 (1ArC), 131.1 (2ArC), 130.88 (=CH), 131.93 (1ArC), 149.81 (1ArC), 153.31 (1ArC), 156.0 (1ArC), 165.79 (C=O), 172.0 (C=O), 191.88 (C=S). HRMS (ES-TOF) *m*/*z* found 617.1109 (M+Na), calculated 617.1805 (M+Na).

*5.1.3.2. (±)-2-((Z)-5-(4-((2-nitrophenylcarbamoyl)methoxy)-3-methoxybenzylidene)-4-oxo-2-thioxo-thiazolidine-3-yl)-3-(4-hydroxyphenyl)propanoic acid (**24**).* Green crystals, 270–273 °C, Yield 60%. FTIR (KBr, cm^{-1}): 3300–2800 (O–H), 3306 (N–H), 3018 (Ar–H), 2933 (AliC–H), 1703 (C=O), 1685 (C=O), 1585 (ArC=C), 1504 (N=O), 1278 (C=S), 1219 (C–O), 1145 (C–N). ^{1}H NMR (500 MHz, DMSO-d_6, δ ppm): 3.40 (bt, 2H, CH_2), 3.90 (s, 3H, CH_3), 4.86 (s, 2H, CH_2), 5.60 (bm, 1H, CH), 7.17–7.41 (m, 6H, ArH), 7.60 (s, 1H, =CH), 7.77 (t, 1H, ArH), 8.10 (d, *J* = 9.5 Hz, 2H, ArH), 8.20 (d, *J* = 9.5 Hz, 2H, ArH), 9.20 (s, 1H, OH), 9.42 (bs, 1H, NH), 10.83 (s, 1H, OH). ^{13}C NMR (500 MHz, DMSO-d_6, δ ppm): 36.0 (CH_2), 56.23 (CH_3), 57.0 (CH), 68.15 (CH_2), 114.36 (1ArC), 114.76 (2ArC), 116.0 (=C), 124.16 (2ArC), 125.0 (2ArC), 124.41 (1ArC), 125.42 (1ArC), 125.91 (2ArC), 127.76 (1ArC), 132.20 (=CH), 132.21 (1ArC), 135.47 (1ArC), 140.15 (2ArC), 149.24 (1ArC), 149.84 (1ArC), 167.41 (C=O), 169.0 (2 × C=O), 196.54 (C=S). LCMS (LC-MSD-Trap-SL) *m*/*z* found 610.1 (M+1), calculated 610.0 (M+1).

*5.1.3.3. (±)-2-((Z)-5-(4-((pyridin-2-ylcarbamoyl)methoxy)-3-methoxybenzylidene)-4-oxo-2-thioxo-thiazolidin-3-yl)-3-(4-hydroxyphenyl) propanoic acid (**25**).* Pale yellow amorphous solid, mp 279–284 °C, Yield 63%. FTIR (KBr, cm^{-1}): 3400–2500 (O–H), 3205 (N–H), 3039 (Ar–H), 2960 (AliC–H), 1708 (C=O), 1676 (C=O), 1535 (C=N), 1508 (ArC=C), 1282 (C=S), 1244 (C–O), 1139 (C–N). ^{1}H NMR (500 MHz, DMSO-d_6, δ ppm): 3.40 (bt, 2H, CH_2), 3.89 (s, 3H, CH_3), 4.95 (s, 2H, CH_2), 5.60 (bm, (α hydrogen) 1H, CH), 6.60 (d, *J* = 8.5 Hz, 1H, ArH), 6.96 (t, *J* = 8.5 Hz, 1H, ArH), 7.12–8.05 (m, 8H, ArH), 7.46 (s, 1H, =CH), 8.34 (d, *J* = 8.5 Hz, 1H, ArH), 9.16 (bs, 1H, OH), 10.50 (s, 1H, NH). ^{13}C NMR (500 MHz, DMSO-d_6, δ ppm): 38.77 (CH_2), 56.10 (CH_3), 67.0 (CH_2), 68.02 (CH), 110.34 (1ArC), 113.24 (1ArC), 115.36 (=C), 120.32 (1ArC), 122.91 (1ArC), 126.05 (1ArC), 128.40 (1ArC), 130.16 (1ArC), 134.57 (=CH), 138.87 (2ArC), 148.62 (2ArC), 149.75 (1ArC), 150.19 (1ArC), 151.72 (1ArC), 135.47 (1ArC), 140.15 (1ArC), 149.24 (1ArC), 156.12 (1ArC), 167.41 (C=O), 173.18 (C=O), 191.87 (C=S). LCMS (LC-MSD-Trap-SL) *m*/*z* found 566.0 (M+1), calculated 566.0 (M+1).

*5.1.3.4. (±)-2-((Z)-5-(4-(benzyloxy)-3-methoxybenzylidene)-4-oxo-2-thioxo-thiazolidin-3-yl)-3-(4-hydroxyphenyl)propanoic acid (**26**).* Yellow amorphous solid, mp 247–251 °C, Yield 69%. FTIR (KBr, cm^{-1}): 3400–2500 (O–H), 3022 (Ar–H), 2960 (AliC–H), 1712 (C=O), 1508 (ArC=C), 1267 (C=S), 1244 (C–O), 1138 (C–N). ^{1}H NMR (500 MHz, DMSO-d_6, δ ppm): 3.40 (bt, 2H, CH_2), 3.84 (s, 3H, CH_3), 5.22 (s, 2H, CH_2), 5.80 (bm, (α hydrogen) 1H, CH), 6.50–7.60 (m, 12H, ArH), 7.53 (s, 1H, =CH), 9.22 (bs, 1H, OH), 10.45 (s, 1H, NH). LCMS (LC-MSD-Trap-SL) *m*/*z* found 522.9 (M+1), calculated 522.0 (M+1).

*5.1.3.5. (±)-2-((Z)-5-(4-((phenylcarbamoyl)methoxy)-3-methoxybenzylidene)-4-oxo-2-thioxo-thiazolidin-3-yl)-3-(4-hydroxyphenyl)propanoic acid (**27**).* Yellow solid, mp 283–286 °C, Yield 61%. FTIR (KBr, cm^{-1}): 3500–3000 (O–H), 3207 (N–H), 3014 (Ar–H), 2929 (AliC–H), 1738 (C=O), 1697 (C=O), 1512 (C=N), 1504 (ArC=C), 1280 (C=S), 1232 (C–O), 1139 (C–N). ^{1}H NMR (500 MHz, DMSO-d_6, δ ppm): 3.40 (bt, 2H, CH_2), 3.91 (s, 3H, CH_3), 4.92 (s, 2H, CH_2), 5.65 (bm, 1H, CH), 6.60–8.20 (m, 12H, ArH), 7.48 (s, 1H, =CH), 9.10 (bs, 1H, OH), 9.87 (s, 1H, NH), 10.90 (s, 1H, OH). ^{13}C NMR (500 MHz, DMSO-d_6, δ ppm): 37.90 (CH_2), 56.19 (CH_3), 56.50 (CH), 68.03 (CH_2), 110.64 (1ArC), 113.70 (2ArC), 115.64 (=C), 124.25 (1ArC), 125.46 (1ArC), 125.87 (2ArC), 125.89 (2ArC), 130.27 (=CH), 131.21 (1ArC), 132.12 (1ArC), 135.41 (2ArC), 140.31 (2ArC), 149.91 (1ArC), 152.41 (1ArC), 156.28 (1ArC), 167.23 (C=O), 169.1 (C=O), 172.0 (C=O), 191.88 (C=S). HRMS (ES-TOF) *m*/*z* found 587.1063 (M+Na), calculated 587.0907 (M+Na).

*5.1.3.6. (±)-5-(4-((phenylcarbamoyl)methoxy)benzylidene)-4-oxo-2-thioxo-thiazolidin-3-yl)-3-(4-hydroxyphenyl)propanoic acid (**28**).* Pale yellow solid, mp 248–251 °C, Yield 63%. FTIR (KBr, cm^{-1}): 3500–2500 (O–H), 3205 (N–H), 3022 (Ar–H), 2929 (AliC–H), 1707 (C=O), 1680 (C=O), 1589 (ArC=C), 1244 (C=S), 1215 (C–O), 1111 (C–N). ^{1}H NMR (500 MHz, DMSO-d_6, δ ppm): 3.40 (bt, 2H, CH_2), 4.85 (s, 2H, CH_2), 5.70 (bm, 1H, CH), 6.60–7.90 (m, 13H, ArH), 7.77 (s, 1H, =CH), 9.23 (bs, 1H, OH), 9.88 (s, 1H, NH), 10.20 (s, 1H, OH). ^{13}C NMR (500 MHz, DMSO-d_6, δ ppm): 37.90 (CH_2), 56.50 (CH), 68.03 (CH_2), 110.64 (1ArC), 113.70 (2ArC), 115.64 (=C), 124.25 (1ArC), 125.46 (1ArC), 125.87 (2ArC), 125.89 (2ArC), 130.27 (=CH), 131.21 (1ArC), 132.12 (1ArC), 135.41 (2ArC), 140.31 (2ArC), 149.91 (1ArC), 152.41 (1ArC), 156.28 (1ArC), 167.23 (C=O), 172.0 (2 × C=O), 191.88 (C=S). HRMS (ES-TOF) *m*/*z* found 557.0092 (M+Na), calculated 557.0901 (M+Na).

5.2. Biological methods

The methods used to evaluate the biological activity of compounds have been reported by us earlier [24,33].

5.2.1. Glucose uptake measurement

Six well microtitre plates with each well capacity of 5 mL (*n* = 4) were selected for the study. Plates were divided into following groups; Group 1: 2 mL of Tyrode solution with 2000 mg/L glucose.

Group 2: 2 mL of Tyrode solution with 2000 mg/L glucose and regular insulin (Nova Nardisk, 40 IU/mL) 5 μL containing 0.2 units of insulin. Groups 3–26: 2 mL of Tyrode solution with 2000 mg/L glucose and 2 mg of the test compound **3–20**, **23–28**. Group 27: 2 mL of Tyrode solution with 2000 mg/L glucose and 2 mg of rosiglitazone (standard). Groups 28–51: 2 mL of Tyrode solution with 2000 mg/L glucose, regular insulin 5 μL containing 0.2 units of insulin and 2 mg of the test compound **3–20**, **23–28**. Group 52: 2 mL of Tyrode solution with 2000 mg/L glucose, regular insulin 5 μL containing 0.2 units of insulin and 2 mg of rosiglitazone (standard). Wistar rats of either sex were maintained on a standard pellet diet, water *ad libitum*, and fasted overnight. The animals were killed by decapitation and diaphragms were taken out swiftly avoiding trauma and divided into two halves. The hemi-diaphragms were then rinsed in cold Tyrode solution (without glucose) to remove any blood clots and transferred to the respective wells. The plates were closed with the lids and incubated for 45 min at 21 °C with shaking at 60 cycles per min. Following the incubation, the glucose content of the incubated wells was measured by GOD/POD enzymatic method using Merckotest glucose kit and Merck-Microlab 200 analyser.

5.2.2. Serum glucose and triglyceride lowering activity

Male Wistar rats weighing between 150 and 200 g were procured from in-house animal facility of J.S.S. college of Pharmacy, Ootacamund. The animals were housed under standard conditions of temperature (22 ± 3 °C) and relative humidity (30–70%) with a 12:12 light:dark cycle. The animals were fed with standard pellet diet (3–5% fat, 68–70% carbohydrate, 18–20% protein, 0.5–1% vitamins and minerals) and water *ad libitum*. The Institutional Animal Ethics Committee (IAEC) of J.S.S. College of pharmacy approved the proposal. Dexamethasone sodium phosphate was obtained as a gift sample from M/S. Strides Arcolabs, Bangalore, India. Triglyceride and glucose estimation kits were from Ecoline, Merck Ltd. Mumbai, India. All the other reagents and chemicals used in the study were of analytical grade. The six compounds that showed activity in *in vitro* screening and rosiglitazone were suspended in 0.5%w/v sodium carboxymethyl cellulose (CMC) at the concentration of 1 mg/mL. These suspensions were administered at a dose volume of 10 mL/kg body weight. As a preliminary study all the synthesized compounds and rosiglitazone were tested at a single dose level of 10 mg/kg, per oral (p.o.). The animals were divided into nine groups, each consisting of six rats, to study the dexamethasone induced insulin resistance and hyperlipidemia (Table 2). All the animals received their assigned treatment daily for a period of 10 days. Rats of groups 2–9 were daily fasted overnight before the dexamethasone treatment [21]. No death of animal was observed in the experimental period. On day 11 the animals were anesthetized with ether and blood was collected from reteroorbital plexus. Serum was then separated for the estimation of glucose and triglyceride using Ecoline triglyceride and glucose estimation kits.

5.2.3. Statistics

All the results were expressed as mean ± SEM and the data was analyzed using one-way ANOVA followed by Dennett's multiple comparison post-test using GraphPad Prism 4 software. P values <0.05 were considered significant.

5.2.4. Histopathology of the liver samples

After collecting blood on day 11, animals were sacrificed under ether anaesthesia and each liver was examined for any grossly visible lesions. Three representative liver samples, each from groups 1, 2, 3, 5 and 6 (Table 2), were selected for the histopathological examination. All the removed-livers were fixed in a formaldehyde solution (which consists of 10 mL formaldehyde, 90 mL distilled water) for a duration of about 90 h. The tissue samples were embedded in paraffin blocks using the standard procedure. Histochemical staining method applied to the 4 μm sections obtained from liver blocks was examined for general tissue composition, by hematoxyline–eosin (H&E). All slides were covered with Canada balsam, and viewed under light microscope with an inbuilt camera attachment for the presence of carcinomas, adenomas or preneoplastic lesions using established criteria. The results are shown in Table 3 [44].

5.2.5. CoMSIA study

The glucose uptake activities of the title compounds were taken forward for the CoMSIA study to define the structure–activity relationships. The test and training set compounds were chosen manually such that low-, moderate-, and high-activity compounds were present in approximately equal proportions in both the sets. The glucose uptake activities were converted into natural log molar antihyperglycemic activity data by dividing the original values by their respective molecular weights and taking natural logarithms, as it would give numerically larger values for the active compounds than those of the inactive compounds ($-\ln$MGU). The training set was designed in such a way so as to account for all the structural and activity variations among the compounds. Twenty compounds were taken in the training set such that they represent each congeneric series of compounds, which spans the 24 compounds. The rest, four compounds constituted the test set or external set to validate the model generated by the CoMSIA study. The common structures of each congeneric series of compounds along with the structure of each compound and their biological activity values are given in Table 1.

The molecular modeling software SYBYL 6.7 installed on a Silicon graphics work station with IRIX 6.5 operating system was used for the three-dimensional structure generation and molecular modeling studies [45]. All the compounds were built from fragments in the SYBYL database. Each structure was fully geometry-optimized using the standard Tripos force field with a distance-dependent dielectric function until a root mean square (rms) deviation of 0.001 kcal/mol Å was achieved [46]. The partial atomic charges, required for the electrostatic interactions, were computed using Gasteiger–Marsili method as implemented in the SYBYL [47].

The conformational search was performed using systematic search protocol. The rotatable bonds in all molecules were searched from 0° to 360° in 10° increments. The minimum energy conformation thus obtained was subsequently used in the analyses.

The important requirement for CoMSIA technique is that the 3D structures of the molecules to be analyzed be aligned according to a suitable conformation template, which is assumed to adopt a "bioactive conformation" [48]. The molecules in the database were aligned using the "Database Align" routine available in SYBYL. The compounds were fitted to the template molecule **24**, one of the most active molecules that correlated with the binding affinity towards PPAR-γ receptor. The alignment rule was optimized by using the appropriate common substructure (phenylalanine connected to the rhodanine ring structure) for the alignment. The aligned training set is shown in Figs. 3–5. Field fit was used to optimize the alignment of molecules to previously calculated fields. These aligned molecules were stored as train aligned and test aligned databases, respectively.

For all steps, the default Sybyl settings were used unless otherwise noted. CoMSIA steric, electrostatic, hydrophobicity, hydrogen bond donor and hydrogen bond acceptor interaction fields were calculated at each 3D cubic lattice intersection point of a regularly spaced grid 2.0 Å in x, y and z directions to encompass the aligned molecules. The steric term (Lennard–Jones 6–12 potential) and electrostatic (Coulomb potential) field interactions were calculated

using the sp^3 carbon probe atom (1.52 Å van der Waals radius) carrying +1 charge, with a distance dependant dielectric at each lattice point. The charges were determined using Gasteiger–Marsili method. The energy calculation was performed for all grid points such that all energies were constrained to be between −30 and 30 kcal/mol.

Partial least squares (PLS) analysis was done to derive the 3D-QSAR models, utilizing the CoMSIA standard scaling for the molecular fields [47]. The activity data (-lnMGA) was used as the dependant variable and the predictive value of the model, represented by the q^2, was evaluated using the leave-one-out (LOO) cross validation method. Column filtering was used to exclude the columns with a variance smaller than 2.0 units, to speed up calculations and to reduce the noise between the calculated columns. The optimum number of components was determined based on the standard error of prediction at different component levels and q^2 values. The conventional r^2 values for training set were also calculated under different combinations of CoMSIA models. Bootstrapping analysis for 100 runs was performed, to further assess the robustness and statistical confidence of the derived models. Bootstrapping involves the generation of many new datasets from the original dataset and is obtained by randomly choosing samples from the original dataset. The statistical calculation is performed on each of these bootstrapping samplings [49]. The difference between the parameters calculated from the original dataset and the average of the parameters calculated from the many bootstrapping samplings is a measure of the bias of the original calculations. Models with a crossvalidation (q2) value above 0.3 were sought, since at this value the probability of chance correlation is less than 5% [43]. The activities of the training set and test set compounds were predicted, to validate and to ensure the developed CoMSIA model. The actual and predicted values of the compounds are listed in Table 1.

The 3D-QSAR models were established for our structures. Graphical examination of the best developed model reveal the areas around the molecules that contain a greater or lesser amount of electronegative groups, electropositive groups, hydrophobic groups, hydrogen bond donors (OH or NH groups), hydrogen bond acceptors (N, O, F) and whether sterics were an important factor for glucose uptake activity.

Acknowledgment

We acknowledge AICTE, New Delhi, for funding this project under research promotion scheme.

References

[1] C.S. Cockram, Diabetes mellitus in the Asia-Pacific region, Hong Kong Med. J. 6 (2000) 43–52.
[2] A.M. Fontbonne, E.M. Eschwege, Insulin and cardiovascular disease, Diabet. Care 14 (1991) 461–469.
[3] M.I. Harris, K.M. Flegal, C.C. Cowie, M.S. Eberhardt, D.E. Goldstein, R.R. Little, H.M. Wiedmeyer, D.D. Byrd-Holt, Prevalence of diabetes, impaired fasting glucose, and impaired glucose tolerance in U.S. adults: the third national health and nutrition examination survey, 1988–1994, Diabet. Care 21 (1998) 518–524.
[4] G.M. Reaven, Banting lecture 1998: role of insulin resistance in human disease, Diabetes 37 (1988) (1988) 1595–1607.
[5] J.P. Anderson Vora, Current concepts of renal: hemodynamics in diabetes, J. Diabet. Complicat. 9 (1995) 304–307.
[6] C. Day, Thiazolidinediones: a new class of antidiabetic drugs, Diabet. Med. 16 (1999) 179–192.
[7] T.M. Wilson, P.J. Brown, D.D. Sterenbatch, B.R. Henke, The PPARs: from orphan receptors to drug discovery, J. Med. Chem. 43 (2000) 527–550.
[8] T. Forst, B. Wilhelm, A. Pfützner, W. Fuchs, U. Lehmann, F. Schaper, M. Weber, J. Muller, T. Konrad, M. Hanefeld, Investigation of the vascular and pleiotropic effects of atorvastatin and pioglitazone in a population at high cardiovascular risk, Diabet. Vasc. Dis. Res. 5 (2008) 298–303.
[9] S.E. Kahn, S.M. Haffner, M.A. Heise, W.H. Herman, R.R. Holman, N.P. Jones, B.G. Kravitz, J.M. Lachin, M.C. O'Neill, B. Zinman, G. Viberti, Glycemic durability of rosiglitazone, metformin, or glyburide monotherapy, N. Engl. J. Med. 355 (2006) 2427–2443.
[10] A.K. McDonough, R.S. Rosenthal, X. Cao, K.G. Saag, The effect of thiazolidinediones on BMD and osteoporosis, Nat. Clin. Pract. Endocrinol. Metab. 4 (2008) 507–513.
[11] H.D. Berlie, J.S. Kalus, L.A. Jaber, Thiazolidinediones and the risk of edema: a meta-analysis, Diabet. Res. Clin. Pract. 76 (2007) 279–289.
[12] S.E. Nissen, K.N. Wolski, Effect of rosiglitazone on the risk of myocardial infarction and death from cardiovascular causes, N. Engl. J. Med. 356 (2007) 2457–2471.
[13] M.A. Peraza, A.D. Burdick, H.E. Marin, F.J. Gonzalez, J.M. Peters, The toxicology of ligands for peroxisome proliferator-activated receptors, Toxicol. Sci. 90 (2006) 269–295.
[14] M. Lehrke, M.A. Lazar, The many faces of PPARgamma, Cell 123 (2005) 993–999.
[15] H. Esterbauer, H. Oberkofler, F. Krempler, W. Patsch, Human peroxisome proliferator activated receptor gamma coactivator 1 (PPARGC1) Gene: cDNA sequence, genomic organization, chromosomal localization, and tissue expression, Genomics 62 (1999) 98–102.
[16] B.M. Forman, P. Tontonoz, J. Chen, R.P. Brun, B.M. Spiegelman, R.M. Evans, 15-Deoxy-delta 12,14-prostaglandin j2 is a ligand for the adipocyte determination factor PPARgamma, Cell 83 (1995) 803–812.
[17] E. Powell, P. Kuhn, W. Xu, Nuclear receptor cofactors in PPARgamma-mediated adipogenesis and adipocyte energy metabolism, PPAR Res. 2007 (2007) 53843.
[18] B.M. Spiegelman, PPAR-gamma: adipogenic regulator and thiazolidinedione receptor, Diabetes 47 (1998) 507–514.
[19] C. Ranjan, R. Ramanujam, Diabetes and insulin resistance associated disorders: disease and the therapy, Curr. Sci. 83 (2002) 1533–1538.
[20] J.M. Nuss, A.S. Wagman, Recent advances in therapeutic approaches to type 2 diabetes, Annu. Rep. Med. Chem. 35 (2000) 211–220 (Chapter 19).
[21] B. Kuhn, H. Hilpert, J. Benz, A. Binggeli, U. Grether, R. Humm, H.P. Maerki, M. Meyer, P. Mohr, Structure-based design of indole propionic acids as novel PPARalpha/gamma co-agonists, Bioorg. Med. Chem. Lett. 16 (2006) 4016–4020.
[22] S. Sundriyal, B. Viswanad, E. Bharathy, P. Ramarao, A.K. Chakraborti, P.V. Bharatam, New PPARgamma ligands based on 2-hydroxy-1,4-naphthoquinone: computer-aided design: synthesis and receptor-binding studies, Bioorg. Med. Chem. Lett. 18 (2008) 3192–3195.
[23] T. Sohda, K. Mizuno, E. Imamiya, Y. Sugiyama, T. Fujita, Y. Kawamatsu, Studies on antidiabetic agents. II. synthesis of 5-[4-(1-methylcyclohexylmethoxy)-benzyl]thiazolidine-2,4-dione (ADD-3878) and its derivatives, Chem. Pharm. Bull. 30 (1982) 3580–3600.
[24] (a) B.R. Prashantha Kumar, M.J. Nanjan, Novel glitazones: design, synthesis, glucose uptake and structure-activity relationships, Bioorg. Med. Chem. Lett. 20 (2010) 1953–1956;
B.R. Prashantha Kumar, B.R. Mukesh Soni, S. Santhosh Kumar, Kuldeep Singh, Mohan Patil, R.B. Nasir Baig, Laxmi Adhikary, Synthesis, glucose uptake activity and structure-activity relationships of some novel glitazones incorporated with glycine, aromatic and alicyclic amine moieties via two carbon acyl linker, Eur. J. Med. Chem. 46 (2011) 835–844.
[25] T. Tomasic, L.P. Masic, Rhodanine as a privileged scaffold in drug discovery, Curr. Med. Chem. 16 (2009) 1596–1629.
[26] (a) L. Wang, F. Kong, C.L. Kokoski, D.W. Andrews, C. Xing, Development of dimeric modulators for anti-apoptotic bcl-2 proteins, Bioorg. Med. Chem. Lett. 18 (2008) 236–240;
(b) D. Hardej, C.R. Ashby Jr., N.S. Khadtare, S.S. Kulkarni, S. Singh, T.T. Talele, The synthesis of phenylalanine-derived c5-substituted rhodanines and their activity against selected methicillin-resistant *Staphylococcus aureus* strains, Eur. J. Med. Chem. 45 (2010) 5827–5832.
[27] B.R. Prashantha Kumar, M.D. Karvekar, L. Adhikary, M.J. Nanjan, B. Suresh, Microwave assisted syntheses of thiazolidine-2,4-dione motif and microwave induced efficient synthesis of 5-benzylidene-thiazolidine-2,4-dione and 5-benzylidine-2-thioxo-thiazolidine-4-one compounds, J. Heterocycl. Chem. 43 (2006) 897–903.
[28] V.L.M. Guarda, M.A. Pereira, C.A. De Simone, J.C. Albuquerque, S.L. Galdino, J. Chantegrel, Synthesis and structural study of arylidene thiazolidine and benzothiazine compounds, Sulfur Lett. 26 (2003) 17–27.
[29] L. Youfu, M. Liang, Z. Hao, C. Lijuan, L. Rui, H. Chunmei, Y. Shengyong, Y. Xia, C. Zhizhi, L. Zicheng, G. Yan, H. Jing, H. Gu, Y. Li, W. Yuquan, Discovery of (Z)-5-(4-methoxybenzylidene)-thiazolidine-2,4-dione, a readily available and orally active glitazone for the treatment of concanavalin a induced acute liver injury of Balb/C mice, J. Med. Chem. 53 (2010) 273–281.
[30] (a) E. Walaas, O. Walaas, Effect of insulin on rat diaphragm under anaerobic conditions, J. Biol. Chem. 195 (1952) 367–373;
(b) R.R. Chattopadhyay, S.K. Sarkar, S. Ganguly, R.N. Banerjee, T.K. Basa, Effect of extract of leaves of *Vinca rosea* Linn. on glucose utilisation and glycogen deposition by isolated rat hemidiaphargm, Ind. J. Physiol. Pharmacol. 36 (1992) 137–138.
[31] J.N. Feige, L. Gelman, L. Michalik, B. Desvergne, Wahli, From molecular action to physiological outputs: peroxisome proliferator-activated receptors are nuclear receptors at the crossroads of key cellular functions, Prog. Lipid Res. 45 (2006) 120–159.
[32] D.P. Rose, J.M. Connolly, Omega-3-fatty acids as cancer chemopreventive agents, Pharmacol. Ther. 83 (1999) 217–244.
[33] B.R. Prashantha Kumar, T.K. Praveen, M.J. Nanjan, M.D. Karvekar, B. Suresh, Serum glucose and triglyceride lowering activity of some novel glitazones

against dexamethasone induced hyperlipidemia and insulin resistance, Ind. J. Pharmacol. 39 (2007) 299–302.
[34] J. Ruzzin, A.S. Wagman, J. Jensen, Glucocorticoid-induced insulin resistance in skeletal muscles: defects in insulin signalling and the effects of a selective glycogen synthase kinase-3-inhibitor, Diabetologia 48 (2005) 2119–2130.
[35] C. Binnert, S. Ruchat, N. Nicod, L. Tappy, Dexamethasone induced insulin resistance shows no gender difference in healthy humans, Diabet. Metab. 30 (2004) 321–326.
[36] R.A. DeFronzo, R.C. Bonadonna, E. Ferrannini, Pathogenesis of NIDDM. A balanced overview, Diabet. Care 15 (1992) 318–368.
[37] G.M. Reaven, The role of insulin resistance in human disease, Diabetes 37 (1988) 1495–1507.
[38] L.I. William, Hepatotoxicity of thiazolidinediones, Exp. Opin. Drug Saf. 2 (2003) 581–586.
[39] R.M. Todd, L.B. Mark, M.B. Steve, Second-generation thiazolidinediones and hepatotoxicity, Ann. Pharmacother. 38 (2004) 1419–1423.
[40] J. Kohlroser, J. Mathai, J. Reichheld, B.F. Banner, H.L. Bonkovsky, Hepatotoxicity due to troglitazone: report of two cases and review of adverse events reported to the United States Food and Drug Administration, Am. J. Gastroenterol. 95 (2000) 272–276.
[41] S. Donald, R.D. Verschoyle, P. Greaves, T.W. Gant, T. Colombo, M. Zaffaroni, R. Frapolli, M. Zucchetti, M. D'Incalci, D. Meco, R. Riccardi, L. Lopez-Lazaro, J. Jimeno, A.J. Gescher, Complete protection by high-dose dexamethasone against the hepatotoxicity of the novel antitumor drug yondelis (ET-743) in the rat, Cancer Res. 63 (2003) 5902–5908.
[42] C. Hui, H. Yong-Wen, L. Wen-Qi, Z. Jing-Hui, Rosiglitazone prevents murine hepatic fibrosis induced by *Schistosoma japonicum*, World J. Gastroenterol. 14 (2008) 2905–2911.
[43] M. Clark, R.D. Cramer III, D.M. Jones, D.E. Patterson, P.E. Simeroth, Comparative molecular field analysis (CoMFA): toward its use with 3D-structuralatabases, Tetrahedron Comput. Methodol. 3 (1990) 47–59.
[44] T. Harada, R.R. Maranpot, A. Enomoto, S. Tamano, J.M. Ward, Changes in the Liver and Gallbladder, ILSI Press, Washington, DC, 1996. pp. 125–201.
[45] SYBYL Molecular Modelling Software, Version 6.7, Tripos Associates Inc., 1669 Hanley Rd., St. Louis, USA, MO 63144–2913.
[46] M. Clark, R.D. Cramer III, O.N. Van, Validation of the general purpose tripos 5.2 force-field, J. Comput. Chem. 10 (1989) 982–1012.
[47] J. Gasteiger, M. Marsili, Iterative partial equalization of orbital electronegativity a rapid access to atomic charges, Tetrahedron 36 (1980) 3219–3228.
[48] R.D. Cramer III, D.E. Patterson, J.D. Bunce, Comperative molecular field analysis (COMFA): effect of shape on binding of steroids to carried protein, J. Am. Chem. Soc. 110 (1988) 5959–5967.
[49] R.D. Cramer III, J.D. Bunce, D.E. Patterson, L.E. Frank, Crossvalidation, bootstrapping, and partial least squares compared with multiple regression in conventional QSAR studies, Quant. Struct. Act. Relat. 7 (1988) 18–25.